Journal of Power Sources 230 (2013) 303–320

Contents lists available at SciVerse ScienceDirect

Journal of Power Sources

journal homepage: www.elsevier.com/locate/jpowsour

Review

Review and advances of direct methanol fuel cells: Part II: Modeling and numerical simulation

Hafez Bahrami, Amir Faghri*

Department of Mechanical Engineering, University of Connecticut, Storrs, CT 06269, USA

HIGHLIGHTS

- A review of the state-of-the-art DMFC modeling studies is provided.
- Studies for water and methanol crossover are discussed.
- A review of enhanced system energy density for DMFCs is presented.
- The challenges and unresolved issues for DMFC modeling are reported.

ARTICLE INFO

Article history:
Received 20 June 2012
Received in revised form
1 November 2012
Accepted 3 December 2012
Available online 12 January 2013

Keywords:
DMFC
High concentration methanol
Methanol crossover
Water crossover

ABSTRACT

The study of direct methanol fuel cells (DMFCs) is a multi-disciplinary science and technology encompassing a variety of sciences, including transport phenomena, material science and electrochemistry. Experimentation is a priceless tool in developing new methods, finding new materials and explaining corresponding phenomena. Along with the experiments, modeling and simulation play a crucial role in providing detailed insights concerning the complex mass, heat and charged particle transport in a DMFC. Modeling is especially important when an experiment is either too expensive to conduct or unable to capture the detailed underlying physics. A comprehensive review of the state-of-the-art modeling studies regarding mass, heat and charge transport in a DMFC is provided. First discussed are the basics of kinetics for electrochemical. It is followed by a description of the differences between various modeling approaches and the most common terminologies in DMFC modeling. A general set of governing equations, along with the corresponding source terms and the constitutive relations, is presented thereafter. A critical review of the most prominent DMFC modeling studies is divided into four topics: (i) water and methanol crossover, (ii) coupled heat and mass transport, (iii) enhanced system energy density, and (iv) start-up and transient operation. The challenges and unresolved issues for DMFC modeling are then reported to conclude the review.

1. Background

A fuel cell, in general, is an electrochemical energy convertor in which a fuel and an oxidizer react at two electrodes, separated by a solid membrane, to convert the chemical energy of the fuel to electrical energy. A DMFC is classified as a low temperature polymer electrolyte membrane fuel cell (PEMFC) that uses liquid or vapor methanol as fuel. Fig. 1 illustrates the operating principles of a DMFC consisting of five main porous layers: anode gas diffusion layer (AGDL), anode catalyst layer (ACL), polymer electrolyte membrane (PEM), cathode catalyst layer (CCL), and cathode gas diffusion layer (CGDL). Fuel fed to the anode diffuses through the AGDL to reach the ACL. The equilibrium half-reaction of methanol oxidation in the ACL is:

$$CO_2 + 6H^+ + 6e^- \leftrightarrows CH_3OH + H_2O \quad (1)$$

During cell operation (as a galvanic cell), Eq. (1) proceeds backwards to produce carbon dioxide, protons and electrons. The reaction in the ACL takes place in a three-phase boundary, comprised of the Pt–Ru catalyst particles, carbon support, and electrolyte (ionomer). The produced electrons transfer through the carbon support to reach the AGDL and the anode current collector. The generated protons transfer through the ACL ionomer phase to the membrane. Note that throughout this review, electrolyte membrane refers to the Nafion® membrane from Dupont,

DOI of original article: http://dx.doi.org/10.1016/j.jpowsour.2012.10.061.
* Corresponding author. Tel./fax: +1 860 486 0419.
E-mail address: faghri@engr.uconn.edu (A. Faghri).

0378-7753/$ – see front matter © 2012 Elsevier B.V. All rights reserved.
http://dx.doi.org/10.1016/j.jpowsour.2012.12.009

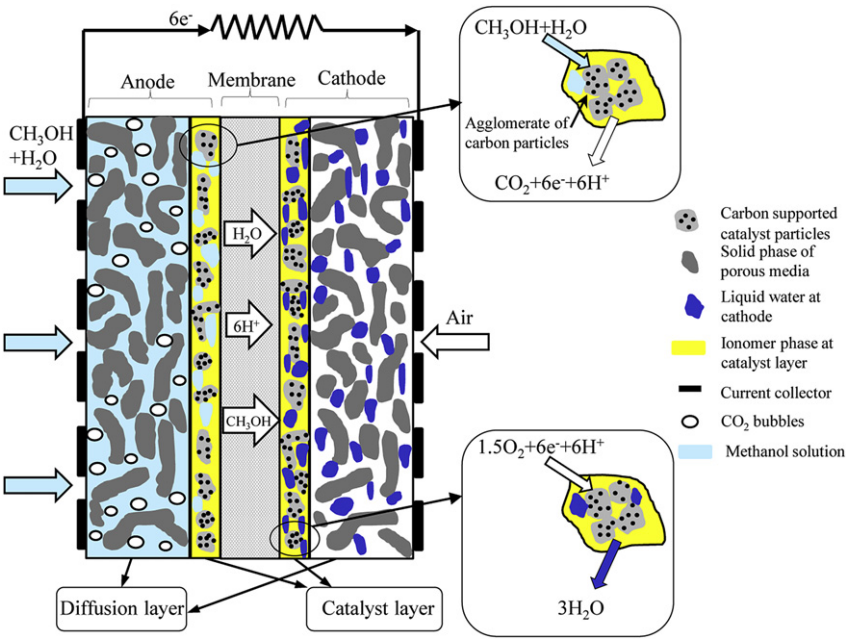

Fig. 1. Schematic of a DMFC during normal operation.

a copolymer of polysulfonyl fluoride vinyl ether and poly(tetrafluoroethylene). The membrane is impermeable to the electron and gaseous species. In the cathode, air diffuses through the CGDL to the CCL, where the oxygen is reduced to heat and water in the presence of electrons and protons. The equilibrium half-cell reaction in the CCL is:

$$\frac{3}{2}O_2 + 6H^+ + 6e^- \rightleftarrows 3H_2O \tag{2}$$

Combining Eqs. (1) and (2) yields the overall galvanic cell reaction as:

$$CH_3OH + \frac{3}{2}O_2 \rightleftarrows 2H_2O + CO_2 \tag{3}$$

It is worthwhile to note that, in terms of the structural compositions, DMFCs are very similar to hydrogen PEMFCs. There are, however, some fundamental differences including the operational condition and the flow regime. In a hydrogen PEMFC, Platinum (Pt) loading of 0.2–0.4 mg cm^{-2} is usually required to achieve the power density of 0.6–0.7 W cm^{-2}. The Platinum–Ruthenium (Pt–Ru) loading in the ACL of a DMFC must be higher, up to 4 mg cm^{-2}, to achieve power densities of 0.05–0.3 W cm^{-2} and of 0.04 W cm^{-2} for active and passive modes of operation, respectively. The relatively higher catalyst loading for DMFCs compensates for the sluggish kinetics of methanol oxidation compared to the hydrogen oxidation in PEMFCs. The other major difference between hydrogen PEMFCs and DMFCs is the two-phase flow regime within the cell. Due to the presence of CO_2 bubbles generated by methanol oxidation in the anode of a DMFC, its two-phase flow effects are more complex than those in a hydrogen PEMFC.

Despite the lower performance of a DMFC compared to a hydrogen PEMFC, the DMFC possesses several prominent advantages, including no need for cooling or humidification of fuel or oxidizer, easy fuel storage and transport, and instant refueling. These features allow DMFCs to be considered as a potentially promising candidate to provide power for a wide range of applications, from transportation to portable devices.

DMFCs are generally classified as either passive or active. In an active DMFC, fuel and oxidizer are forced into the anode and cathode, respectively. This type of DMFC is more suitable for transportation applications, where high power output is required and there is less concern regarding the available space for auxiliary devices. Passive DMFCs, on the other hand, contain no moving parts and are more suitable for portable applications. The primary focus for passive DMFCs is achieving higher system-level energy density in Wh L^{-3} along with improving the power density in W cm^{-2}.

2. Electrochemistry

A fundamental understanding of kinetics and the corresponding thermodynamics is essential for DMFC modeling. In this section, the polarization curve, a common tool to evaluate the cell overall performance, and various voltage losses in the cell are briefly described. Reaction kinetics and deviation from thermodynamic equilibrium are discussed, thereafter.

2.1. Polarization curve

Reactions represented by Eqs. (1)–(3) are in equilibrium and the net flow rates of the reactants and products are zero. According to the basic principles of thermodynamics, the anode and cathode equilibrium half-cell potentials at standard conditions (25 °C and 1 atm) are obtained based on the change in standard Gibbs free energy ($\overline{G}$) for the corresponding half-cell reaction:

$$V_a^{eq} = \frac{-\Delta\overline{G}_a}{6F} = 0.016\,V \quad \& \quad V_c^{eq} = \frac{-\Delta\overline{G}_c}{6F} = 1.229\,V \tag{4}$$

V_a^{eq} and V_c^{eq} are the equilibrium half-cell potentials for the anode and cathode, respectively, and F is the Faraday constant. The overall cell equilibrium potential is $V_c^{eq} - V_a^{eq} = 1.213$ V, which is very close to the equilibrium potential of a hydrogen PEMFC, 1.23 V, at standard conditions.

The cell equilibrium potential corresponds to zero current density. In practice, an external potential – associated with some losses (overpotentials) – is required in order to drive the half-cell reactions into a specific direction and generate/consume the flow of electrons and protons. One of the basic methods to analyze the

corresponding non-equilibrium losses in the anode and cathode reactions is utilizing the Butler–Volmer relation for the galvanic half-cell reactions of Eqs. (1) and (2). A polarization curve, represented by the cell voltage versus current density, is more common in the fuel cell community. In a polarization curve, the anode and cathode losses are added together and the information regarding each half-cell is lost. General information concerning the cell performance and various losses within the system are provided by a polarization curve.

There are three types of losses (overpotentials) that can be tracked in a polarization curve: activation, ohmic and mass transport losses, all of which are illustrated in Fig. 2. Activation loss, the major contributor to the cell voltage loss at lower current densities, is the potential required to drive the reaction from the equilibrium conditions. Due to the sluggish kinetics of methanol oxidation (Eq. (1)), the anode activation loss might be slightly higher than that of the oxygen reduction (Eq. (2)) [1]. Ohmic loss is defined as the potential loss as the electric charges (electrons or ions) flow through a medium. In DMFCs, ohmic loss mainly stems from the ionic (H^+) transport in the catalyst and membrane layers. The electron conductivity of the gas diffusion layer (GDL), $O(1000\ \Omega^{-1}\ m^{-1})$, is nearly two orders of magnitude greater than the proton conductivity of the membrane, $O(10\ \Omega^{-1}\ m^{-1})$. Thus, the ohmic loss caused by electron transport is usually neglected. Mass transport loss is the third type of loss in DMFCs, owing to the lack of reactants in the catalyst sites. It becomes remarkably significant at high current densities, where the excessive demand for reactants at catalyst sites cannot be met. In Fig. 2, 600 A m^{-2} is the limiting current density where the concentration of either oxygen in the CCL or methanol in the ACL is significantly reduced. The corresponding mass transport loss becomes the dominant voltage loss, once the current density approaches the limiting current density.

2.2. Kinetics

Kinetics discusses the electrochemical reaction rates for non-equilibrium conditions. The fundamentals of kinetics for electrochemical reactions are provided in Ref. [2]. Two common kinetics modeling approaches in a DMFC are explained, here. First, the Butler–Volmer equation and the Tafel assumption are described as the most fundamental and basic models for electrochemical kinetics. Non-Tafel kinetics is presented, thereafter.

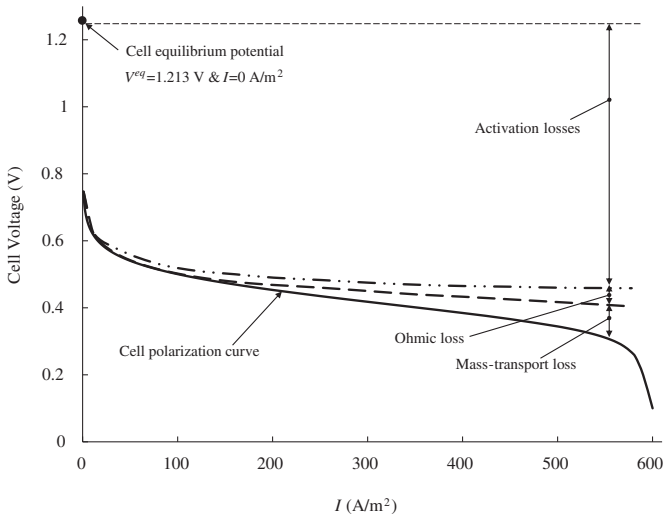

Fig. 2. A representative schematic of a polarization curve.

2.2.1. Butler–Volmer model of kinetics

The kinetics of both the anode and cathode reactions can be explained by the Butler–Volmer model. For a generic equilibrium electrochemical reaction of

$$O + e^- \rightleftarrows R \tag{5}$$

Arrhenius equation may be used to present the forward or backward reaction rate constant (k, $m^2\ s^{-1}$):

$$k = A \cdot \exp\left(\frac{-E_A}{R_u T}\right) \tag{6}$$

where A is the frequency factor, $m^2\ s^{-1}$, T is the temperature, K, R_u represents the universal gas constant, J $K^{-1}mol^{-1}$, and E_A is the activation energy, J mol^{-1}. Implementing the fundamental concept of activation overpotentials into the Arrhenius equation and neglecting the mass transport limit [2], the kinetics of Eq. (5) is described by the following Butler–Volmer relation:

$$J = aJ_o\left[\exp\left(-\frac{\alpha_c F}{R_u T}\eta\right) - \exp\left(\frac{\alpha_a F}{R_u T}\eta\right)\right] \tag{7}$$

where a is the electrochemically active area per unit catalyst volume, m^{-1}, J is the reaction rate, A m^{-3}, J_o denotes the exchange current density, A m^{-2}, η refers to the overpotential, V, and α is the transfer coefficient. Subscripts a and c denote the anodic (backward, $\eta > 0$) and cathodic (forward, $\eta < 0$) reactions of Eq. (5), respectively. In Eq. (7):

$$\alpha_a + \alpha_c = 1 \tag{8a}$$

$$\eta = V - V^{eq} \tag{8b}$$

Tafel kinetics refers to the condition when the reaction Eq. (5) moves in a preferential direction so that one of the terms on the right hand side of Eq. (7) is much smaller than the other. Tafel kinetics for the oxygen reduction reaction (ORR) is obtained by including the mass-transport considerations [2] and assuming negligible oxidation (backward) reaction of Eq. (2), as follows:

$$J_{O_2} = \alpha J_{o,O_2} \cdot \left(\frac{C_{O_2}}{C_{O_2}^{ref}}\right) \cdot \exp\left(-\frac{\alpha_c F}{R_u T}\eta_c\right) \tag{9}$$

where C is the concentration at the reaction sites, mol m^{-3}, and superscript ref denotes a reference value. The Tafel kinetics for the ORR in a DMFC is widely accepted [3–10]. Apart from the frequent utilization of Tafel kinetics for the methanol oxidation reaction (MOR) [3–5,7,11–17], it is not a well appropriate assumption for the sluggish MOR. The Tafel kinetics of the MOR is obtained in a similar manner to Eq. (9), as follows:

$$J_{MeOH} = aJ_{o,MeOH} \cdot \left(\frac{C_{MeOH}}{C_{MeOH}^{ref}}\right) \cdot \exp\left(\frac{\alpha_a F}{R_u T}\eta\right) \tag{10}$$

Note that although the anodic reaction rate in Eq. (7) is negative, from the mass transport modeling perspective, the absolute value of the rate matters. For the rest of this review both anodic and cathodic rates, A m^{-3}, are assumed positive.

Before embarking on the non-Tafel kinetics for MOR, it is imperative to recognize the relation between the overpotential (η) and the phase potentials. Fig. 3 provides a conceptual illustration of the overpotential by differentiating the local potential distributions for the equilibrium ($I = 0$ A m^{-2}) and non-equilibrium ($I \neq 0$ A m^{-2}) conditions. Electrode potential is denoted by ϕ_c and the membrane

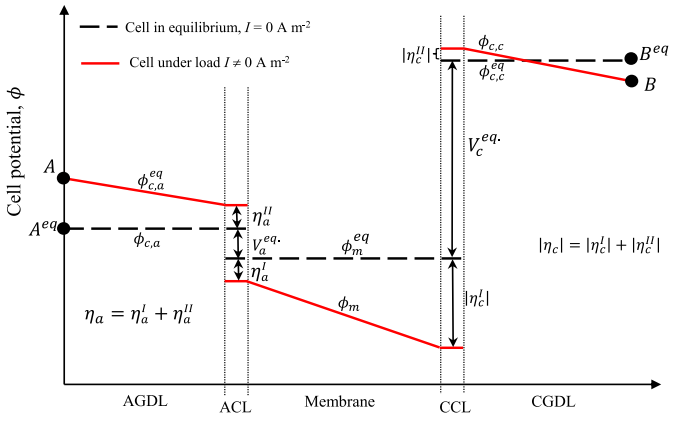

Fig. 3. A representative schematic of potential distributions for a DMFC in equilibrium ($I = 0$ A m^{-2}) and non-equilibrium ($I \neq 0$ A m^{-2}) conditions.

potential is represented by ϕ_m. It is assumed that no methanol crosses through the membrane. When the cell is under equilibrium conditions, all of the potential lines are horizontal, representing no voltage loss (dashed lines in Fig. 3). The overall cell equilibrium voltage is defined as the electrode potential (ϕ_c) difference between two ends of the cell, i.e. between points A and B in Fig. 3. The equilibrium cell voltage (V_{cell}^{eq}) is:

$$V_{cell}^{eq} = \phi_{c,c}|_{B^{eq}} - \phi_{c,a}|_{A^{eq}} = V_c^{eq} - V_a^{eq} = 1.213\ \text{V} \tag{11}$$

However, when the cell is under a load, ($I \neq 0$ A m^{-2}), the potential experiences losses as the electrons and protons flow through the corresponding transport medium (continuous lines in Fig. 3). Anode and cathode overpotentials in the catalyst layers are defined as:

$$\eta_c = -(\phi_{c,c} - \phi_m - V_c^{eq}) \tag{12a}$$

$$\eta_a = -(\phi_{c,a} - \phi_m - V_a^{eq}) \tag{12b}$$

2.2.2. Non-Tafel kinetics for methanol oxidation

Non-Tafel kinetics is the terminology commonly used when the reaction is studied through a set of multi-step reactions. Butler–Volmer kinetic model is still used for each individual step. Various sets of MOR multi-step reaction are reported [18–22]. Nordlund and Lindbergh [20] and Meyers and Newman [19] independently studied the multi-step MOR suggested by Hamnett [23] and Gasteiger et al. [24], respectively, in order to develop an appropriate non-Tafel MOR kinetics. The method of treating the methanol adsorption on the Pt surface was the difference between two models. The adsorption reaction was assumed in equilibrium by Nordlund and Lindbergh [20], while Meyers and Newman [19] assumed that the reaction continues in one direction to form adsorbed methanol on the Pt surface. The most common non-Tafel kinetic for MOR is obtained by considering the following elementary and intermediate reactions [19,22]:

$$CH_3OH_{Reservoir} \rightarrow CH_3OH_{ACL} \tag{13a}$$

$$CH_3OH_{ACL} + Pt \rightarrow CH_3OH_{ad,Pt} \tag{13b}$$

$$CH_3OH_{ad,Pt} \rightarrow CO_{ad,Pt} + 4H^+ + 4e^- \tag{13c}$$

$$H_2O + Ru \leftrightarrow OH_{ad,Ru} + H^+ + e^- \tag{13d}$$

$$CO_{ad,Pt} + OH_{ad,Ru} \rightarrow CO_2 + H^+ + e^-\ Pt + Ru + \tag{13e}$$

where the subscript ad represents adsorption to the corresponding catalyst surface. Using the Butler–Volmer relation for each step above, assuming a dilute methanol solution and performing some mathematical manipulations, the widely used non-Tafel kinetics of MOR is obtained as follows [19,22]:

$$J_{MeOH} = \alpha J_{o,MeOH} \frac{C_{MeOH}}{C_{MeOH} + \Gamma \exp\left(\frac{\alpha_a F}{R_u T}\eta\right)} \exp\left(\frac{\alpha_a F}{R_u T}\eta\right) \tag{14a}$$

where the kinetic constant, Γ, is [22]:

$$\Gamma = K \exp\left(\frac{\alpha_a F}{R_u T} V_a\right) \tag{14b}$$

where K is calculated based on the reaction rate constant of Eqs. (13c) and (13e).

Comparing the Tafel and non-Tafel kinetics of Eqs. (10) and (14a) reveals that a non-Tafel kinetics provides a meaningful concentration dependency for the MOR kinetics which is $C_{MeOH}/(C_{MeOH} + \Gamma \exp(\alpha_a F\eta/R_u/T))$. Tafel kinetics linearly relates the reaction rate to the methanol concentration by provoking a reference value, C_{MeOH}^{ref}, which must be fitted by experimental data.

3. Methodologies

The purpose of this section is twofold: first, to present a summary of major macroscopic DMFC models demonstrating their distinct features in a table and then to provide a brief, yet comprehensive, description of various DMFC modeling methodologies and the most frequently used terminologies.

Table 1 summarizes the main features of the major DMFC macroscopic numerical models organized in the order of the publication year. The first column of the table shows the model dimension. The next three columns describe whether the model considers transient, non-isothermal, and two-phase flow characteristics or not. It is followed by a column about the two-phase flow modeling approach, which can be either multi-fluid multiphase (MFM) or multiphase mixture (M^2). The constitutive diffusion equation employed for each phase is outlined in the next two columns. The eighth column explains whether the model is using Darcy's law or the Navier–Stokes equations for the conservation of momentum in the porous layers. The MOR kinetics is shown in the next column. The tenth column points out the inclusion of the chemical equilibrium in the model. The eleventh column explains whether the numerical model considers the whole cell as one computational domain or as multiple domains related by matching fluxes at the interfaces. The following column addresses the inclusion of the charge transport equation in the model. Column thirteen indicates the phase of the fuel fed to the anode. The next two columns indicate the feeding modes to the cathode and anode (active or passive). The last two columns remark the inclusion of dissolved water in ionomer phase and the incorporation of the Leverett equation, respectively. In the following, various modeling approaches, briefly presented in Table 1, are explained.

3.1. Macroscopic versus microscopic models

Macroscopic models are continuum and based on the averaging of transport variables over a control volume large enough compared to the microstructure. They treat the catalyst layer and the GDL as macro-homogeneous porous layers. A macroscopic

Table 1
Features of the most important numerical models of DMFCs.

Investigators	1D/2D/3D	Steady/Transient	Isothermal/Non-isothermal	Single/Two-phase modeling	Two phase-modeling	Gas phase diffusion	Liquid phase diffusion	Darcy/N.S.	MOR kinetics	Chemical equilibrium/non-equilibrium	Single/Multi-domain	Solving charge transport	Vapor-/Liquid-feed	Air supply	Fuel supply	Water diffusion through the membrane	Leverett eq.
Baxter et al. 1999 [164]	1	St.[a]	Is.[b]	Sin.[c]	N/A[d]	F.[f]	F.	N/A	B.V.[h]	N/A	N/A	Y[k]	L.[l]	N/A	N/A	Y	N/A
Dohle et al. 2000 [145]	1	St.	Is.	Sin.	N/A	S.M.[f]	N/A	N/A	Ta.[h]	N/A	M.D.[j]	Y	V.[l]	A.[m]	A.	Y	N/A
Kolikovsky 2000 [123]	2	St.	Is.	Sin.	N/A	S.M.	F.	D.[g]	Ta.	N/A	M.D.	Y	L.	A.	A.	N	N/A
Kolikovsky et al. 2000 [165]	2	St.	Is.	Sin.	N/A	S.M.	N/A	D.	Ta.	N/A	M.D.	Y	V.	A.	A.	N	N/A
Meyers Newman 2002 [19,121,144]	1	St.	Is.	Sin.	N/A	S.M.	S.M.	N/A	N.T.[h]	N/A	S.D.[j]	Y	L.	N/A	N/A	Y	N/A
Nordlund and Lindbergh 2002 [20]	1	St.	Is.	Sin.	N/A	N/A	S.M.	N/A	M.S.[h]	N/A	N/A	Y	L.	N/A	N/A	Y	N/A
Divisek et al. 2003 [62]	2	Tr.[a]	N.I.[b]	Two[c]	MFM[e]	S.M.	N/A	D.	M.S.	N.E.[i]	S.D.	Y	L.	A.	A.	N	N
Murgia et al. 2003 [63]	1	St.	Is.	Two	MFM	S.M.	F.	D.	Ta.	N.E.	M.D.	Y	L.	A.	A.	N	N
Wang and Wang 2003 [7]	2	St.	Is.	Two	M^2	F.	F.	D.	Ta.	Eq.[i]	M.D.	N[k]	L.	A.	A.	N	Y
Birgersson et al. 2003 [50]	2	St.	Is.	Sin.	N/A	N/A	F.	D.	N.T.	Eq.	M.D.	N	L.	N/A	A.	N	Y
Birgersson et al. 2004 [49]	2	St.	Is.	Two	M^2	F.	F.	D.	N.T.	Eq.	M.D.	N	L.	N/A	A.	N	Y
Ge and Liu 2006 [167]	3	St.	Is.	Sin.	N/A	F.	F.	N.S.[g]	Ta.	N/A	M.D.	N	L.	A.	A.	N	N/A
Danilov et al. 2006 [51]	3	St.	Is.	Two	M^2	F.	F.	D.	Ta.	Eq.	M.D.	Y	L.	A.	A.	N	Y
Rice and Faghri 2006 [8]	2	Tr.	Is.	Two	MFM	S.M.	F.	D.	N.T.	N.E.	S.D.	Y	L.	P.[m]	P.	N	Y
Vera 2007 [188]	3/1	St.	Is.	Sin.	N/A	F.	F.	N.S.	N.T.	N/A	M.D.	N	L.	A.	A.	N	N/A
Liu and Wang 2007 [53]	3	Tr.	Is.	Two	M^2	F.	F.	N.S.	N.T.	Eq.	S.D.	Y	L.	A.	A.	Y	Y
Liu and Wang 2007 [73]	3	Tr.	Is.	Two	M^2	F.	F.	N.S.	N.T.	N/A	S.D.	Y	L.	A.	A.	Y	Y
Liu and Wang 2007 [52]	1	St.	Is.	Two	M^2	F.	F.	D.	N.T.	Eq.	N/A	Y	N/A	N/A	N/A	N/A	Y
Ge and Liu 2007 [54]	3	St.	Is.	Two	M^2	F.	F.	N.S.	Ta.	Eq.	M.D.	N	L.	A.	A.	N	Y
Yang and Zhao 2007 [4]	2	St.	Is.	Two	MFM	F.	F.	D.	Ta.	N.E.	M.D.	N	L.	A.	A.	N	Y
Yang and Zhao 2007 [3]	2	St.	Is.	Two	MFM	F.	F.	D.	Ta.	N.E.	M.D.	N	L.	A.	A.	N	Y
Yang et al. 2007 [15]	3	St.	Is.	Two	MFM	F.	F.	D.	Ta.	N.E.	M.D.	N	L.	A.	A.	N	Y
Yan and Jen 2008 [55]	2	St.	Is.	Two	M^2	F.	F.	N.S.	B.V.	Eq.	S.D.	N	L.	A.	A.	N	Y
Xu et al. 2008 [6]	1	St.	Is.	Two	MFM	F.	F.	D.	Ta.	N.E.	M.D.	N	L.	P.	P.	Y	Y
Chen et al. 2008 [68]	2	St.	N.I.	Two	MFM	F.	F.	D.	Ta.	N.E.	M.D.	Y	L.	P.	P.	N	Y
Xiao and Faghri 2008 [58]	2	Tr.	N.I.	Two	MFM	S.M.	F.	D.	N.T.	Eq.	S.D.	Y	L.	P.	P.	N	Y
Rice and Faghri 2008 [9]	1	Tr.	N.I.	Two	MFM	S.M.	F.	D.	N.T.	Eq.	S.D.	Y	V.	P.	P.	N	Y
Rice and Faghri 2008 [10]	2	Tr.	N.I.	Two	MFM	S.M.	F.	D.	N.T.	Eq.	S.D.	Y	L.	P.	P.	N	Y
Yang and Zhao 2008 [14]	2	Tr.	Is.	Two	MFM	F.	F.	D.	N.T.	N.E.	M.D.	N	L.	P.	P.	N	Y
Yang et al. 2008 [5]	2	St.	Is.	Two	MFM	F.	F.	D.	N/A	N.E.	M.D.	Y	L.	P.	P.	Y	Y
Xiao and Faghri 2009 [57]	2	Tr.	N.I.	Two	MFM	S.M.	F.	D.	N.T.	Eq.	S.D.	Y	V	P.	P.	N	Y
Xu and Faghri 2009 [13]	2	St.	N.I.	Two	MFM	F.	F.	D.	Ta.	N.E.	M.D.	N	L.	P.	P.	Y	N
Xu and Faghri 2009 [11]	2	St.	N.I.	Two	MFM	F.	F.	D.	Ta.	N.E.	M.D.	N	L.	P.	P.	Y	Y
Xu and Faghri 2009 [12]	2	St.	N.I.	Two	MFM	F.	F.	D.	Ta.	N.E.	M.D.	N	V.	P.	P.	Y	Y
Xiao et al. 2009 [56]	2	Tr.	N.I.	Two	MFM	S.M.	F.	D.	N.T.	Eq.	S.D.	Y	L.	P.	P.	N	Y
Yang and Zhao 2009 [65]	2	St.	Is.	Two	MFM	F.	F.	D.	Ta.	N.E.	M.D.	N	L.	P.	P.	Y	Y
Shaffer and Wang 2009 [59]	1	St.	Is.	Two	M^2	F.	F.	D.	N.T.	Eq.	M.D.	N	L.	P.	P.	Y	Y
Yang and Zhao 2009 [65]	2	St.	Is.	Two	MFM	F.	F.	D.	Ta.	N.E.	M.D.	N	L.	P.	P.	Y	Y
Bahrami and Faghri 2010 [16]	2	St.	N.I.	Two	MFM	F.	F.	D.	Ta.	N.E.	M.D.	N	L.	A.	P.	N	Y
Bahrami and Faghri 2010 [67]	2	Tr.	N.I.	Two	MFM	S.M.	F.	D.	N.T.	N.E.	S.D.	Y	L.	P.	P.	Y	Y
Shaffer and Wang 2010 [74]	1	St.	Is.	Two	M^2	F.	F.	D.	N/A	Eq.	M.D.	N	L.	P.	P.	Y	Y
Miao et al. 2010 [70]	2	St.	N.I.	Two	MFM	F.	F.	D.	N.T.	N.E.	M.D.	Y	L.	A.	A.	N	Y
Bahrami and Faghri 2011 [17]	2	St.	N.I.	Two	MFM	F.	F.	D.	Ta.	N.E.	M.D.	N	L.	P.	P.	Y	Y

(*continued on next page*)

Table 1 (*continued*)

Investigators	1D/2D/3D	Steady/Transient	Isothermal/Non-isothermal	Single/Two-phase modeling	Two phase-modeling	Gas phase diffusion	Liquid phase diffusion	Darcy /N.S.	MOR kinetics	Chemical equilibrium/non-equilibrium	Single/Multi-domain	Solving charge transport	Vapor-/Liquid-feed	Air supply	Fuel supply	Water diffusion through the membrane	Leverett eq.
Xu and Faghri 2011 [69]	2	St.	N.I.	Two	MFM	F.	F.	D.	Ta.	N.E.	M.D.	N	L.	P.	A.	Y	Y
Yang et al. 2011 [64]	2	St.	Is.	Two	MFM	F.	F.	D.	Ta.	N.E.	M.D.	N	V.	P.	P.	Y	Y
Garvin and Meyer 2011 [61]	1	St.	Is.	Two	MFM	S.M.	S.M.	N/A	N/A	Eq.	S.D.	N	L.	N/A	P.	N/A	N/A
Bahrami and Faghri 2012 [66]	2	Tr.	N.I.	Two	MFM	S.M.	F.	D.	N.T.	N.E.	S.D.	Y	V.	P.	P.	Y	N
He et al. 2012 [71]	2	St.	N.I.	Two	MFM	F.	F.	D.	Ta.	N.E.	M.D.	Y	L.	P.	P.	Y	Y

[a] St/Tr refers to steady/transient.
[b] Is./N.I. refers to isothermal/non-isothermal.
[c] Sin/Two refers to single/two phase.
[d] N/A refers to not applicable or not available.
[e] MFM/M^2 refers to multi-fluid multiphase and multiphase mixture modeling of two-phase flow.
[f] F./S.M. refers to Fick's/Maxwell–Stefan diffusion equations.
[g] D./N.S. refers to Darcy's law/Navier–Stokes equation.
[h] B.V./Ta./N.T./M.S. refers to Butler–Volmer/Tafel/non-Tafel/multi-step methanol oxidation kinetics.
[i] N.E./Eq. refers to non-equilibrium/equilibrium condition.
[j] M.D/S.D. refers to multi/single computational domain.
[k] Y/N refers to yes/no.
[l] L/V refers to liquid-/vapor-feed DMFC.
[m] A./P. refers to active/passive DMFC.

model is considered to be the most feasible and economical tool to investigate the transport phenomena at the system level. Various macroscopic formulations and assumptions are explained in the subsequent sections. Note that there are some weaknesses associated with the macroscopic approach. Macroscopic modeling of flow in DMFC porous medium is usually described by the classical Darcy law. The Darcy law is easy to use but requires the knowledge of the effective properties such as porosity, permeability, tortuosity, conductivity and capillary pressure. Measurement of these effective properties is challenging when it comes to very thin and non-self-supported layers. Due to the macroscopic nature, they cannot capture the effect of structural morphology of the catalyst layer and the GDL on the underlying two-phase physics. There are few correlations, such as capillary pressure as functions of relative permeability and liquid water saturation, for the two-phase models. Current macroscopic two-phase models for DMFCs mostly employ a capillary pressure relation based on the Leverett function, originally developed for a geologic, hydrophilic porous medium.

Microscopic and meso-scale models focus on the pore level transport phenomena of either the catalyst layer or the GDL, based on an idealized network representing the porous medium using a distribution function for pore size and porosity. For the catalyst layers, the agglomerate model and pore network model (PNM) are two pore-scale approaches. In the agglomerate model, the catalyst layer is described by a porous medium made of agglomerates of size 100–1000 nm, each of which contains couple of carbon supported Pt particles with a typical size of 30 nm. An analytical solution of the transport phenomena in the agglomerate scale is then coupled with the macroscopic model [4,25–33]. This approach allows capturing the effect of parameters such as agglomerate size, catalyst loading and the thickness of the electrolyte around the agglomerate on the transport phenomena and the cell performance. The flow between agglomerates is solved by the Darcy law. In the other approach for the catalyst layers, species, electrons and protons transport between network passages consisting of the voids between agglomerates in the catalyst layer is considered by a PNM. The PNMs are developed for both single [34,34] and two-phase flow [35] in the CCL. Unlike hydrogen PEMFCs, handling the two-phase flow in the CCL is crucial for DMFCs, as significant amount of liquid water exists due to either the electrochemical reaction or employing a water management layer (WML) in the cathode. PNM is also used to provide an in-depth and fundamental understanding of water transport dynamics in the micro-porous structure of the GDL [36–46]. It can be used for other purposes, such as evaluating the effective diffusivity of species through the GDL [47] and ice formation dynamics in the GDL during cold start-up [48]. Note that PNM requires tremendous computational and time resources, which is the major disadvantage of this method. As noted earlier, the focus of this review is only macroscopic modeling of DMFCs.

3.2. Equilibrium versus non-equilibrium models

In the macroscopic two-phase DMFC modeling, two common approaches are used to account for the mass transfer between phases based on the equilibrium and non-equilibrium assumptions.

3.2.1. Equilibrium approach

Equilibrium approach assumes that the two phases in the system come into a thermodynamic equilibrium. This assumption allows the calculation of the gaseous species mole/mass fraction based on the mole/mass fraction of that species in liquid phase. To reach the thermodynamic equilibrium, the following three conditions must be fulfilled: (1) *thermal equilibrium*, identical temperatures of two phases, (2) *mechanical equilibrium*, no pressure

difference between two phases, and (3) *chemical equilibrium*, the same chemical potential for two phases. When two phases come into chemical equilibrium, the instantaneous mass flux from the liquid to the gas phase equals the mass flux from the gas to the liquid phase. Representative DMFC models incorporating the equilibrium assumption are [7,9,10,49–61].

In the case of thermodynamic equilibrium, Raoult's or Henry's law may be used to calculate the saturation pressure of each individual species in a solution. Each of these two laws applies to the extreme ends of the composition range of a solution. According to the Raoult's law, the equilibrium vapor pressure of the component in large excess in the solution (such as water in a very dilute methanol solution) is proportional to its molar fraction in the liquid phase, and the proportionality constant is the vapor pressure of the pure substance. For instance, the equilibrium water vapor pressure in a dilute methanol solution is:

$$p^{\mathrm{eq}}_{\mathrm{v,H_2O,solution}} = p^{\mathrm{eq}}_{\mathrm{v,H_2O,pure}} \cdot x_{\mathrm{l,H_2O}} \tag{15}$$

On the other hand, according to Henry's law, the vapor pressure of the solute (methanol in a very dilute solution) is also proportional to its molar fraction in the liquid phase. Unlike the Raoult's law, the proportionality constant needs to be experimentally measured (Henry's constant). For example, the vapor pressure of methanol in a dilute methanol solution is calculated by Henry's law, as follows:

$$p^{\mathrm{eq}}_{\mathrm{v,MeOH,solution}} = \kappa_{\mathrm{H}}^{\mathrm{MeOH,H_2O}} \cdot x_{\mathrm{l,MeOH}} \tag{16}$$

3.2.2. Non-equilibrium approach

Non-equilibrium approach employs empirical correlations to consider the mass loss/gain due to phase change of condensable species, i.e. water and methanol in a DMFC [3–6,8,12–17,25,62–71]. The condensation rate of water and methanol is obtained by the following relations [3,72]:

$$\dot{m}^{\mathrm{m}}_{\mathrm{i,H_2O}} = \left(\frac{M_{\mathrm{H_2O}} k_{\mathrm{c}} \varepsilon (1-s) x_{\mathrm{g,H_2O}}}{2R_{\mathrm{u}}T} \left(1 + \frac{\left| p_{\mathrm{g,H_2O}} - p^{\mathrm{sat}}_{\mathrm{g,H_2O}} \right|}{p_{\mathrm{g,H_2O}} - p^{\mathrm{sat}}_{\mathrm{g,H_2O}}} \right) + \frac{k_{\mathrm{e}} \varepsilon s p_{\mathrm{l}}}{2} \left(1 - \frac{\left| p_{\mathrm{g,H_2O}} - p^{\mathrm{sat}}_{\mathrm{g,H_2O}} \right|}{p_{\mathrm{g,H_2O}} - p^{\mathrm{sat}}_{\mathrm{g,H_2O}}} \right) \right) \left(p_{\mathrm{g,H_2O}} - p^{\mathrm{sat}}_{\mathrm{g,H_2O}} \right) \tag{17}$$

$$\dot{m}'''_{\mathrm{l,MeOH}} = A_{\mathrm{lg}} h_{\mathrm{lg}} (1-s) s \frac{\left(p_{\mathrm{g,MeOH}} - p^{\mathrm{sat}}_{\mathrm{g,MeOH}} \right)}{R_{\mathrm{u}}T} M_{\mathrm{MeOH}} \tag{18}$$

where k_{c} ($\mathrm{s^{-1}}$) and k_{e} ($\mathrm{Pa^{-1}\ s^{-1}}$) are the condensation and evaporation rates, respectively, h_{lg} is the interfacial transfer rate constant for methanol, m $\mathrm{s^{-1}}$, and A_{lg} denotes the interfacial specific area between liquid and gas phases, $\mathrm{m^2\ m^{-3}}$.

3.3. Multi-fluid multiphase (MFM) versus mixture multiphase (M^2) model

As shown in the sixth column of Table 1, the macroscopic, Eulerian-averaged equations for multiphase flow in DMFCs are tackled by two different, but equivalent, formulations: (i) the MFM model [3–6,8–10,12–17,25,56–58,62–71], and (ii) the M^2 model [7,49,51–55,59,73,74]. In the MFM approach, the averaging is performed for each individual phase within the system. For a two-phase system, two sets of continuity, momentum and energy equations for each phase describe the transport phenomena. The M^2 model is an equivalent derivation of the MFM model intending to decrease the number of governing equations by adding equations of all phases until they resemble the single-phase transport formulation. The major advantage of the M^2 model over the MFM model is that in the M^2 model one single set of equations for continuity, momentum and energy is enough to describe the system. The most commonly used M^2 model appropriate for the flow field in the porous media of DMFCs is developed by Wang and Cheng [75–77]. A comprehensive description of both approaches is provided by Faghri and Zhang [78].

Though the reduced number of governing equations and simpler numerical implementation are two attractive features of the M^2 model, the model does not capture the mutual effects of species in a multi-component system. The M^2 model is based on the Fickian diffusive flux of species. It also assumes the local chemical equilibrium at phase interface. The model is therefore not appropriate when the non-equilibrium effects between phases are of importance, such as the two-phase transport phenomena inside a vapor-feed DMFC.

A conceptual example is provided here in order to illustrate the differences between two above referenced formulations in a computational control volume for a one-dimensional two-phase flow, consisting of two condensable species, *water* and *methanol*. As depicted in Fig. 4, the MFM model considers a system with two phases consisting of four original species. Considering the overall continuity equation for each phase, *two species equations* are

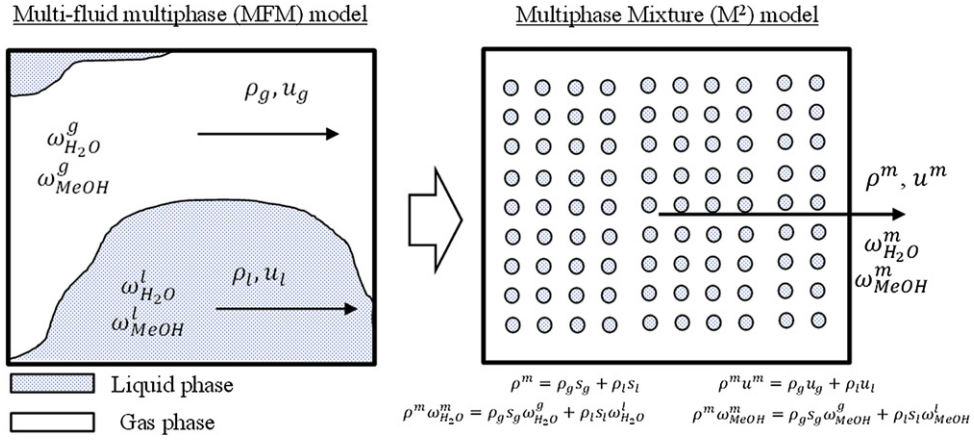

Fig. 4. A comparison of the MFM model where two phases are separately taken care of, and the M^2 model where a single fluid with new transport properties is assumed.

required to have a well-posed description of the system. The M^2 model, on the other hand, represents the system as a single fluid with new transport properties and two newly defined species, i.e. $\omega^{m}_{H_2O}$ and ω^{m}_{MeOH}, as follows:

$$\rho^{m}\omega^{m}_{MeOH} = \rho_g s_g \omega^{g,eq}_{MeOH} + \rho_l s_l \omega^{l,eq}_{MeOH} \quad (19a)$$

$$\rho^{m}\omega^{m}_{H_2O} = \rho_g s_g \omega^{g,eq}_{H_2O} + \rho_l s_l \omega^{l,eq}_{H_2O} \quad (19b)$$

$$\rho^{m} = \rho_g s_g + \rho_l s_l \quad (19c)$$

where the superscript m denotes the M^2 model. The overall mixture species conservation requires $\sum_i \omega^{m}_i = 1$, implying that only *one mixture species equation* must be solved in the M^2 model rather than two. Post-processing is required to calculate the original species values. Based on the chemical equilibrium assumption in the M^2 model, the gas phases are considered to be saturated. The mass fraction in the gas phase is therefore a function of that in the liquid phase:

$$\omega^{g,eq}_{H_2O} = f\left(\omega^{l,eq}_{H_2O}\right) \quad (20a)$$

$$\omega^{g,eq}_{MeOH} = f\left(\omega^{l,eq}_{MeOH}\right) \quad (20b)$$

The equilibrium binary phase diagram and Henry's or Raoult's law (Eqs. (15) and (16)) are used to find the function above. It is also known that:

$$\omega^{g,eq}_{MeOH} + \omega^{g,eq}_{H_2O} = 1 \quad (21a)$$

$$\omega^{l,eq}_{MeOH} + \omega^{l,eq}_{H_2O} = 1 \quad (21b)$$

One mixture species equation along with the post-processing Eqs. (19)–(21) is enough to obtain all original species in the system, as well as the liquid saturation, s_l.

3.4. Models based on mass fraction versus those based on concentration

There are two classes of models available for DMFCs. In some of them, species equations are described based on the mass fraction (ω_i, kg kg^{-1}) [7–10,16,17,52,53,56–58,66,67,73], while in others the species equations appear in terms of molar concentration (C_i, mol m^{-3}) [3–6,12–15,25,64,65,68–71]. In order to describe the differences between these two approaches, two averaged velocities for a mixture composed of N components is defined. If V_i is the velocity of the ith species, then the mass-averaged (V) and molar-averaged ($\widehat{V}$) velocities are defined as:

$$V = \sum_{i=1}^{N} \omega_i V_i \quad \& \quad \widehat{V} = \sum_{i=1}^{N} x_i V_i \quad (22)$$

where x_i is the molar fraction of species i in the mixture. Based on the above definitions, the mass and molar fluxes of the mixture are:

$$\dot{m}'' = \sum_{i=1}^{N} \dot{m}''_i = \rho V \quad \& \quad \dot{n}'' = \sum_{i=1}^{N} \dot{n}''_i = C\widehat{V} \quad (23)$$

The species equations are written based on either mass fraction or molar concentration:

$$\rho_k \frac{\partial \omega_{k,i}}{\partial t} + \rho_k \nabla\cdot\left(\omega_{k,i}\cdot V_k\right) = \rho_k \nabla\cdot\left(D_{ij}\nabla\omega_{k,i}\right) + \dot{m}'''_i \quad (24)$$

$$\frac{\partial C_{k,i}}{\partial t} + \nabla\cdot\left(C_{k,i}\cdot\widehat{V}_k\right) = C_k \nabla\cdot\left(D_{ij}\nabla x_{k,i}\right) + \dot{n}'''_i \quad (25)$$

where subscripts i and j denote the component index in the solution and subscript k pertains to phase k. If the appropriate mass- and molar-averaged velocities are provided for Eqs. (24) and (25), both approaches will yield equivalent results.

Since the mass-averaged velocity is the most convenient basis for the continuity, momentum, and energy equations, it would be much easier to use the species equations based on the mass fraction rather than molar fraction or molar concentration. The other advantage of mass fraction based formulation is explained in terms of conservativeness. While the total number of moles is not necessarily conserved in a reactive system, the species and mixture masses are preserved quantities. The relation between ω_i and x_i is:

$$\omega_i = \frac{x_i M_i}{\sum x_i M_i} \quad (26)$$

The two types of velocities shown in Eq. (22) are identical only when the molar weight of all species in the mixture is equal, which is not the case in a DMFC. Mass-averaged velocity is utilized in most DMFC models in which species equations are based on molar concentration, [3,5,6,14,15]. Therefore, a slight deviation in the results due to this assumption is expected.

4. Governing equations

A DMFC model is comprised of six conservation equations: mass, momentum, species, charge, energy, and dissolved water content in the ionomer, which can be formulated by either the MFM or M^2 approach. The former is chosen to be presented here. While the mass, momentum, and species equations are written for each individual phases, the energy equation is based on the assumption that the gas and liquid phases are of identical temperature. All transport equations are highly coupled through non-linear source terms, and fall into the following generalized conservative form:

$$\frac{\partial(\rho\psi)}{\partial t} + \nabla\cdot(\rho V\psi) = \nabla\cdot(\Gamma\nabla\psi) + S \quad (27)$$

where Γ is the diffusion coefficient, S is the source term, ψ denotes the dependent variable to be solved, ρ is the density, and V is the velocity vector.

Table 2 summarizes the above noted conservation principles, along with the source terms at various layers. Darcy's law is used to represent the momentum equation which, in combination with the continuity equation, results in the pressure equation for each phase [67]. The multi-component, Maxwell–Stefan relation is introduced for the gas species diffusive transport. Source terms corresponding to the phase change and electrochemical reactions are respectively identified by lat and reac superscripts.

The two-phase flow inside the porous media of a DMFC is classified as capillary pressure driven flow. The most common empirical relation for the capillary pressure is based on the Leverett function, $J(s)$:

$$p_c = p_g - p_l = \sigma\cos(\theta)\left(\frac{\varepsilon}{k}\right)^{0.5} J(s) \quad (28)$$

As noted earlier, the Leverett function, $J(s)$, is a function of liquid saturation, wettability and morphological properties of the porous

Table 2
Governing equations with the corresponding source terms in various regions, based on the MFM formulation.

		Source terms		
		Diffusion layers	Catalyst layers	Membrane
Pressure, liquid	$\partial(\overline{\rho_l})/\partial t = \nabla\cdot(D_{p,l}^{eff}\nabla p_l) + \dot{S}_{p,l}$	$+\sum \dot{S}_{m,i}^{lat}$	$+\sum(\dot{S}_{m,i}^{lat} + \dot{S}_{m,l,i}^{reac}) + \dot{S}^{osm}$	$\dot{S}^{osm}$
Pressure, gas	$\partial(\overline{\rho_g})/\partial t = \nabla\cdot(D_{p,g}^{eff}\nabla p_g) + \dot{S}_{p,g}$	$-\sum \dot{S}_{m,i}^{lat}$	$-\sum(\dot{S}_{m,i}^{lat} - \dot{S}_{m,g,i}^{reac})$	
Species, liquid i = MeOH	$\partial(\overline{\rho_l}\omega_{l,i})/\partial t + \nabla\cdot(\overline{\rho_l}V_l\omega_{l,i}) = \nabla\cdot(D_{l,MeOH}^{eff}\nabla\omega_{l,i}) + \dot{S}_{l,i}$	$\dot{S}_{m,i}^{lat}$	$\dot{S}_{m,i}^{lat} + \dot{S}_{m,l,i}^{reac}$	
Species, gas i = O_2, CO_2, H_2O, MeOH	$\partial(\overline{\rho_g}\omega_{g,i})/\partial t + \nabla\cdot(\overline{\rho_g}V_g\omega_{g,i}) = \nabla\cdot(D_{g,ii}^{Stef-Max}\nabla\omega_{g,i}) + \dot{S}_g$	$-\dot{S}_{m,i}^{lat} + \dot{S}_{m,i}^{Stef-Max}$	$-\dot{S}_{m,i}^{lat} + \dot{S}_{m,l,i}^{reac} + \dot{S}_{m,i}^{Stef-Max}$	
Energy	$\partial(\overline{\rho C}T)/\partial t + \nabla\cdot(\overline{\rho C}VT) = \nabla\cdot(k_T^{eff}\nabla T) + \dot{S}_T$	$\dot{S}_T^{lat}$	$J(\eta - T\Delta\bar{S}/6F) + \dot{S}_T^{lat}$	I^2/σ_{mem}^{eff}
Charge, electron	$0 = \nabla\cdot(\sigma_e\nabla\phi_c) + \dot{S}_e$		$-J_{ox} + J_{red}$	
Charge, proton	$0 = \nabla\cdot(\sigma_{mem}\nabla\phi_{mem}) + \dot{S}_{mem}$		$+J_{ox} - J_{red}$	
Dissolved water in ionomer	$\partial(\varepsilon\rho_{H_2O})/\partial t = \nabla\cdot(D_{dw}\nabla C_{dw}M_{H_2O}) + \dot{S}_\lambda$			$\dot{S}_\lambda^{mem}$

where

$\overline{\rho_l} = \varepsilon s\rho_l$, $\overline{\rho_g} = \varepsilon(1-s)\rho_g$, $D_{p,l}^{eff} = \rho_l\frac{k_{rl}K}{\mu_l}$, $D_{p,g}^{eff} = \rho_g\frac{k_{rg}K}{\mu_g}$, $D_{l,i}^{eff} = \rho_l D_{l,i}\varepsilon^{1.5}s^{1.5}$, $k_{rl} = s^3, k_{rg} = (1-s)^3$, $\overline{V_l} = \varepsilon s V_l$, $\overline{V_g} = \varepsilon(1-s)V_g$, $\overline{\rho C} = \overline{\rho_g}C_{p,g} + \overline{\rho_l}C_{p,l} + (1-\varepsilon)\rho_s C_{p,s}$,

$\overline{\rho CV} = \overline{\rho_g}C_{p,g}V_g + \overline{\rho_l}C_{p,l}V_l$, $k_T^{eff} = \varepsilon s k_l + \varepsilon(1-s)k_g + (1-\varepsilon)k_{DL/CL}$, $\dot{S}^{osm} = -\nabla\cdot(n_d M_l I/F)$, $\dot{S}_\lambda^{mem} = \nabla\cdot\left(\omega_{l,H_2O}\cdot\left(D_{p,l}^{eff}\nabla P_l\right) - n_{d,H_2O}M_{H_2O}I/F\right)$, $\dot{S}_i^{lat} = \dot{m}_{l,i}'''$, $\dot{S}_i^{reac} = \frac{c_i j}{nF}M_i$,

$\dot{S}_i^{Max-Stef} = \nabla\cdot\left(\sum_{\substack{j=1\\ j\neq i}}^{4} D_{g,ij}^{Max-Stef}\nabla\omega_{g,j}\right)$, $D_{g,ij}^{Max-Stef} = (\varepsilon(1-s))^{1.5}\rho_g B_{g,ij}^{eff}$, $D_{g,ii}^{Max-Stef} = (\varepsilon(1-s))^{1.5}\rho_g B_{g,ii}^{eff}$, $\dot{S}_T^{lat} = \sum \dot{m}_{l,i}'''h_{fg,i}$, $B_{ii} = \overline{M}\left[\omega_i/M_N/D_{iN} + \sum_{\substack{k=1\\ k\neq i}}^{N}(\omega_k/M_k/D_{ik})\right]$,

$B_{ij} = -\overline{M}\,\omega_i\left[1/M_j/D_{ij} - 1/M_N/D_{iN}\right]$

material. Udell's correlation [79], obtained from geological porous media, is adopted to evaluate the Leverett function:

$$J(s) = \begin{cases} 1.42(1-s) - 2.12(1-s)^2 + 1.26(1-s)^3 & \text{if } \theta < 90^\circ \\ 1.42s - 2.12s^2 + 1.26s^3 & \text{if } \theta > 90^\circ \end{cases} \quad (29)$$

There have been efforts to develop more appropriate empirical capillary pressure correlation for the mixed-wet porous structure of fuel cells [62,80–85]. Mixed-wet refers to the coexistence of hydrophilic and hydrophobic pores in the porous structure. Xu and Faghri provided a review of all capillary pressure relations developed for the fuel cell modeling [13].

5. Transport phenomena

There have been numerous DMFC models developed since the 1990s. These models provided the fundamental understanding of coupled heat-species-charge transport phenomena in a DMFC. The theme of all DMFC models centers in dealing with one or a few key issues, including: (1) methanol and water crossover, (2) coupled heat and mass transfer, (3) low system energy density, and (4) start-up and the transient operation. This section is organized to provide a critical review of DMFC models based on these key issues.

5.1. Crossover

Methanol and water crossover account for the major concerns in developing DMFC technologies. In the following, water and methanol crossover and their interrelation will be discussed.

5.1.1. Methanol crossover

As shown in Fig. 1, methanol is prone to transport through the membrane by three mechanisms: *electroosmosis*, in which methanol molecules stick to the H^+-ions in ionomer phase, *diffusion*, where the gradient of the dissolved methanol concentration in the ionomer phase is the driving force and *convection*, which is caused by the pressure difference within the membrane.

Back in late 80s, when DMFCs were at the early stage of being considered as a candidate for power supply, Verbrugge [86] calculated the diffusion of methanol through Nafion® 117 membrane. Verbrugge noted that the diffusion rate of methanol crossover through the membrane can be as fast as that through water. Diffusion rate of 1.15×10^{-9} m^2 s^{-1} was reported at 25 °C. Due mostly to the high methanol diffusivity through Nafion® and, in part, to the cost of this type of membrane, there have been investigations in either modifying the Nafion® [87–94] or providing cheaper synthesis of substitute polymers [95–100]. Despite all these efforts, Nafion® is still the most feasible membrane for a DMFC in terms of availability, stability (thermal, chemical, and physical) and proton conductivity. Using Nafion®, nearly 30–40% of methanol might cross through the membrane, causing significant reduction in both fuel utilization efficiency and cell power density [101,102].

Experimental studies for methanol crossover were mostly focused on: (1) capturing the influences of operating conditions, such as anode feed methanol concentration, current density, temperature, cathode pressure, anode methanol flow rate in the anode channel [103–107], (2) studying the effect of membrane parameters [104,108–110], and (3) investigating the effect of the anode structure [103,111–114]. Along with the experimental studies, the proposed physical models made a significant improvement in the fundamental understanding of key parameters influencing the methanol crossover over the past decade, ranging from analytical [22,86,115–120] to numerical, complex models [3,4,6–8,10,17,49,52,62,63,67,68,115,116,121–124]. The prediction capabilities are evaluated from two perspectives: (i) validation against the experimentally measured methanol crossover, and (ii) capturing the fundamental physics of methanol reaction in the CCL and its effect on the cell performance.

Despite rapid improvement in the prediction capabilities of DMFC models, there are few investigations reporting a comparison between the experimental measurements and the mathematically predicted methanol crossover [63,118–121,125]. Meyer and Newman [121] predicted methanol crossover in agreement with the experimental measurements, for 0.25 M $< C_{MeOH,res} <$ 10 M. Scott et al. [118] reported a good agreement between the experimental measurements and the predictions from a one-dimensional, single-phase model over a moderate current density of 3000–4000 A m^{-2}

for 1 M methanol feed in the anode and pure oxygen pressure of 1, 2 and 3 bar in the cathode. Murgia et al. [63] demonstrated an acceptable agreement between the experimental results and the predictions from a one-dimensional, two-phase model for methanol feed concentrations of 0.5, 1 and 1.5 M. The main assumptions in their model were zero differential gas pressure in the porous medium, a fully saturated membrane, and liquid phase transport of reactants in the anode. Eccarius et al. [119] validated the analytical predictions of methanol crossover with the experimental results by some non-validated adjustments in the electroosmotic drag coefficient and the methanol concentration in the ACL. Rosenthal et al. [120] reported an analytical model whose predictions of methanol crossover as a function of temperature and methanol feed concentration were in good agreement with the experimental measurements. Exchange current density and kinetic transfer coefficient were reported as the only fitted variables. Methanol crossover aggravates as the temperature and methanol feed concentration increase (Fig. 5) [7,120], and decreases when the membrane gets thicker. As depicted in Fig. 5 for moderate methanol feed concentrations (<3 M), methanol crossover versus the current density is decreasing [3,4,120,121], while other studies report an initial increase followed by a decreasing methanol crossover with current density [1]. The trend is, however, different for higher methanol feed concentrations (≳3 M) and the methanol crossover increases with current density [121]. The different patterns of methanol crossover versus current density are explained via the methanol concentration in the ACL. Methanol crossover occurs mostly through the electroosmosis which linearly depends on the methanol concentration in the ACL. For low feed methanol concentrations, as current density increases, the methanol concentration in the ACL and consequently the electroosmotic drag of methanol to the cathode reduce. However, if the methanol feed concentration is high enough to maintain sufficient methanol in the ACL (≳3 M), methanol crossover via electroosmosis never decreases with current density. Note also that, in both cases, diffusive transport of methanol through membrane to the cathode also depends on methanol concentration in the ACL.

Despite all of the above referenced advancements in prediction of the experimentally measured methanol crossover, the available two-phase models are generally unable to accurately match the experimental results without fitting some parameters. This is mainly due to some uncertainties in specifying boundary conditions, constitutive closure relation (such as capillary relation) and the inability to resolve the influence of the structural morphologies. For instance, the convective (and diffusive) crossover of methanol is a strong function of liquid saturation at the catalyst layers which, in turn, depends on the capillary pressure relation and the specified liquid saturation boundary condition.

Methanol crossover influences the cell performance in three ways: (i) imposing extra overpotential due to the reaction of methanol with oxygen in the CCL, known as the mixed potential, (ii) reducing the oxygen concentration in the CCL and thereby increasing the oxygen reduction overpotential, and (iii) catalyst (Pt) poisoning in the CCL.

The majority of DMFC models only consider the effect of the reduced oxygen concentration in the CCL on the cathode overpotential, attributed to the methanol–oxygen reaction [3–7,11,14–17,49,50,59,126]. However, calculations show that this mechanism alone cannot explain losses, which are generally in the order of several hundred mV [52]. There are few investigations in understanding the fundamentals of the overpotential imposed on the cathode by the reaction of methanol in the CCL [26,52,127,128]. Liu and Wang [52] applied a one-dimensional, M^2 model to the cathode of a DMFC to elucidate the mixed potential in the CCL. The competition of methanol and oxygen for specific catalyst sites and catalyst poisoning phenomena were disregarded. Kulilovsky [128] provided an analytical model for the methanol oxidation in the CCL and reported that the methanol–oxygen reaction in the CCL decreased the local oxygen concentration in the electrode, and thereby raised the local overpotential. Tamaki et al. [26] considered the simultaneous influences of mixed potential in the CCL and the CO poisoning of the Pt catalyst by a cylindrical agglomerate model. Both numerical predictions and experiments showed that the cathode mixed overpotential increased sharply at a certain methanol crossover flux, depending on the Pt loading of the CCL. Fig. 6 depicts the cathode mixed potential as a function of methanol crossover flux to the cathode (I_p). It is shown that implementing the cathode Pt poisoning by the methanol oxidation into the DMFC models is of significant importance. The cathode Pt loading also has a crucial effect on the cathode mixed overpotential. For a lower Pt loading, catalyst poisoning results in a sharp increase in the cathode mixed overpotential at a certain methanol crossover flux. Despite these advancements in understanding the physics behind the mixed overpotential, further research must be conducted to provide more detailed insight regarding the simultaneous competition of oxygen and methanol for specific Pt surface and the poisoning effects.

5.1.2. Water crossover

In a fashion similar to methanol, water is also prone to cross through the membrane by three mechanisms: *electroosmosis*, *diffusion*, and *convection*. Dealing with water crossover in a DMFC is usually referred to "*water management*". Water management in

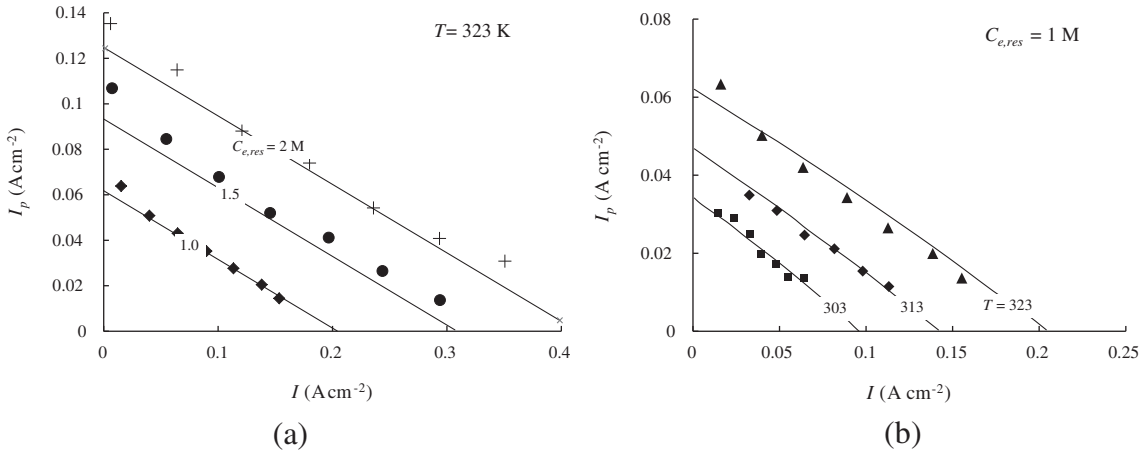

Fig. 5. Methanol crossover (I_p) as a function of (a) methanol concentration in the reservoir and (b) the cell temperature (Nafion® 117). Adopted from Ref. [120].

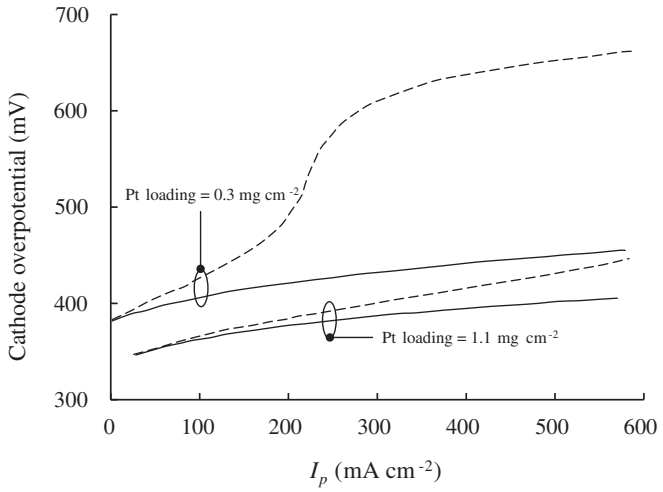

Fig. 6. Cathode overpotential versus the methanol crossover rate for considering (dashed line) and neglecting (continuous line) the catalyst poisoning effect for two Pt loadings in the CCL. Adopted from Ref. [26].

hydrogen PEMFCs stands for a balance between the membrane hydration and the cathode flooding. The problem is however more challenging for a DMFC particularly for the passive operation. Water management in a DMFC refers to providing water for the anode, while preventing the cathode flooding. Unlike hydrogen PEMFCs, membrane hydration is not an issue in DMFCs as long as water is provided for the anode reaction. In this section, the requirement of dilute methanol solution in the ACL is first addressed. Major parameters influencing the water crossover in a DMFC are discussed, thereafter. Water diffusion through membrane, practical methods of water management and the interrelation between the water management and the methanol crossover are then described.

Equation (2) states that the oxidation of 1 mol of methanol requires 1 mol of water. However, in practice, the ratio of the number of moles of water to that of methanol is much higher than one and a very dilute methanol solution is required. A tremendous quantity of water crosses through the membrane from the anode to the cathode. If the electroosmosis, with a typical drag coefficient of 2.5, is the only effective mechanism of the water crossover, approximately 2.5 × 6 mol of water migrate to the cathode corresponding to 6 mol of generated protons for each mole of methanol in the ACL. Thus, in a DMFC with five basic porous layers, shown in Fig. 1, 16 mol of water are roughly needed for each mole of reacting methanol in the ACL. As a result, a very dilute methanol solution must be fed by the supply. The need for a very dilute methanol solution significantly reduces the energy density of the system, a major concern for portable applications. Considering 15 mol of water migrated to the cathode and 3 mol of water produced by ORR in the CCL, a large amount of water exists at the cathode side, potentially causing flooding. Experimental studies confirm that the cathode flooding is mostly due to the water crossover, rather than the water production in the ORR [129–131]. The reduced system energy density and cathode flooding are the specific focus of the water management in a DMFC.

Many factors may affect the water crossover through the membrane, such as temperature, membrane thickness, current density, and operating pressure. As the temperature increases, the diffusion coefficient and electroosmotic drag coefficient get higher and, in turn, more water crosses through the membrane [17,113,130–135]. Experimental measurements have shown that as the DMFC temperature increased from 30 to 70 °C, the water crossover flux increased nearly eight times [130]. The effect of membrane thickness on the water crossover depends primarily on the cell structure. For a cell without a WML in the cathode where mostly water diffusion occurs from the anode to cathode, the water crossover increases for thinner the membrane (Fig. 7) [65,129,130,136]. If the water diffusion is directed from the cathode to the anode, for instance, by adding a WML in the cathode, a thinner membrane results in lower water crossover from the anode to the cathode [113,133,135]. Cell current density is a major factor influencing the water crossover in a DMFC. Fig. 8 illustrates that the total water crossover increases with current density as a result of significant increase in the electroosmotic drag and slight reduction in the diffusive transport [6,17]. With increasing current density, more CO_2 in the ACL results in a reduction in the water content of the anode side of the membrane, while more water production in the CCL leads to an increase in the water content of the cathode side of the membrane, leading to a reduction in water diffusion from the cathode to the anode. Convective transport of water, from the cathode to anode, slightly increases with increasing current density mainly due to increased liquid pressure in the CCL. However, the electroosmotic drag, the dominant water transport mechanism from the anode to the cathode, linearly scales with the current density, resulting in more total water crossover.

Fundamental understanding of water distribution and transport across the membrane is required for an accurate modeling. The focus of the available models for the water transport through membrane ranges from the membrane itself [137–143] to the entire membrane electrode assembly of a DMFC [6,17,59,65,144]. The underlying physics for water transport in the Nafion® membrane is still controversial. There are models suggesting the hydraulic permeation (electroosmosis and convection) as the main water transport mechanism in the membrane [140,141], while some others propose the diffusion [142]. Weber and Newman [143] have developed a model that proposes coexisting diffusive and permeation-based transport, based on pore-expansion due to liquid pressure in connective nano-pores within the ionomer. Nonetheless, diffusion is most likely the dominant water transport mechanism through Nafion® in a DMFC, since a dilute methanol solution is usually fed to the anode [6,65].

Modeling of water diffusion through the membrane is one of the most challenging subjects. This is most likely why many DMFC models assumed a fully hydrated membrane with no water diffusion mechanism [3,4,7–10,15,16,49,50,56–58,63]. This assumption

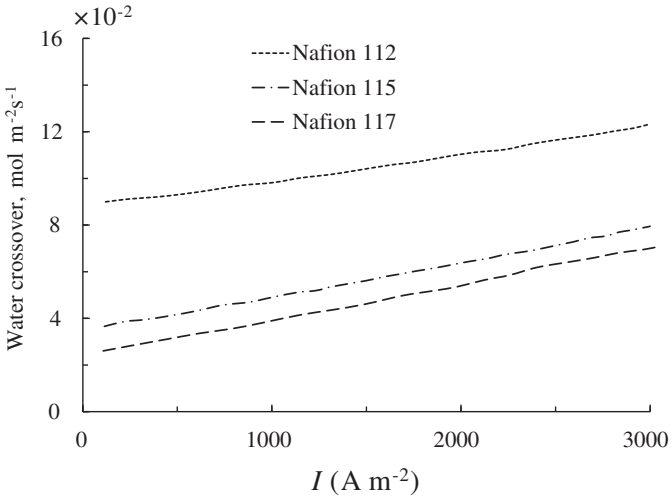

Fig. 7. The effect of membrane thickness on total water crossover through the membrane in a DMFC with five basic porous layers shown in Fig. 1. Adopted from Ref. [65].

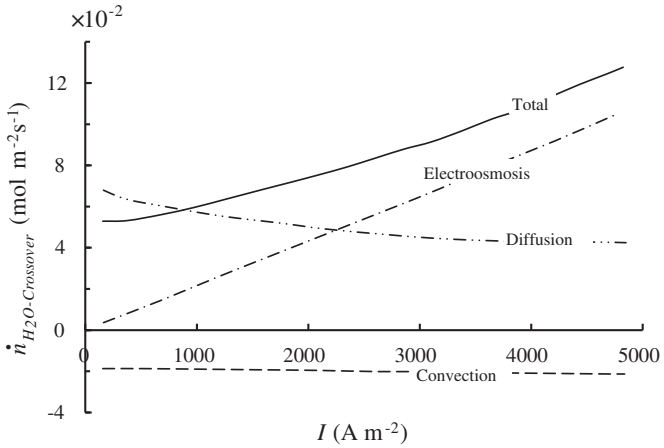

Fig. 8. Various water crossover mechanisms through Nafion®-115 versus current density. Adopted from Ref. [6].

leads to a miscalculation of the water crossover. Three phases of water can potentially exist in the catalyst layer: liquid water, water vapor, and dissolved water in the electrolyte around the agglomerates in the catalyst layers. Two approaches for the modeling of the diffusive water transport through the membrane are distinguishable by equilibrium or non-equilibrium assumption between the dissolved water in the membrane phase and water vapor/liquid in the catalyst layers. Due to the ease of implications in the system-level models, several DMFC models incorporated the equilibrium condition between all water phases in the catalyst layers [11,13,17,53,67,73,142,145], similar to the hydrogen PEMFC models [142,146–150]. The dilemma for this approach is how to account for the coexistence of liquid and vapor phases at the catalyst layers of a DMFC. Experimental data is available for the water content (λ) of the membrane in which the dissolved water is in equilibrium with the liquid water or with the water vapor. The water content is the ratio of the number of moles of water attached to 1 mol of sulfonic acid of the membrane. In a real situation, both liquid and vapor water exist in catalyst layers. Most DMFC models utilize a linear interpolation to account for the presence of both phases of water (liquid and vapor) at the membrane/catalyst interface in order to obtain the water content at the membrane boundaries [11,13,17,53,67,73,142,145]:

$$\lambda_{\text{two-phase}} = \lambda_{\text{v}} + (\lambda_{\text{l}} - \lambda_{\text{v}})s \tag{30}$$

where subscripts v and l stand for vapor and liquid phases of water, respectively, and s is the liquid saturation in the catalyst layer. Equilibrium condition, noted above, might not be achieved instantly [151,152]. Therefore, the finite mass transfer rate between vapor and membrane phase liquid water within the catalyst layers should be accounted for. As both liquid and vapor water co-exist in the catalyst layers under the normal operation of a DMFC, a more realistic and non-equilibrium model to consider the water dissolution in the membrane phase is developed by Shah et al. [153,154]. In the proposed model, three-phase of water, i.e. liquid, vapor and dissolved water in the membrane, are considered. The evaporation and condensation between liquid and vapor along with the adsorption and desorption between dissolved phase and liquid or vapor were included in the model to account for the finite-rate interfacial mass transport. Xu et al. [6] employed the same method to analyze the water transport through the membrane phase by all three water transport mechanisms.

Employing a porous layer, termed as a WML in the preceding sections, either in the cathode or in the anode has attracted the most attention for the water management in a DMFC due in part to easy implementation, an acceptable performance and the cost concerns. If a cathode WML is utilized, high liquid pressure in the cathode is built up upon increasing the hydrophobicity and reducing the WML pore size, and water back-flows to the anode. Peled et al. [155] and Blum et al. [156] reported that the use of a highly hydrophobic cathode WML makes it possible to have water-neutral operating conditions for a DMFC with low methanol feed concentration. Employing the anode WML is another potential method to control water crossover. Liu et al. [157] studied the effectiveness of an anode WML on water crossover in a DMFC. It was reported that the wettability of the anode WML is important in controlling the water crossover. The MEA with a hydrophobic anode WML led to more reduction in water crossover compared to a hydrophilic one. Shaffer and Wang [59] employed a one-dimensional, two-phase model to investigate the importance of using an anode WML to decrease the water for MEAs using the high concentration solutions of methanol. A parametric study was performed to show that a thicker anode WML with a higher hydrophobicity and a lower permeability is more effective in reducing the water and methanol crossover. Later, they extended the model to investigate the function of the anode WML in a DMFC using pure methanol [74]. Yang and Zhao [65] investigated the water transport in a DMFC by incorporating both anode and cathode WML, simultaneously. It was reported that optimum design of the anode porous structure reduces the diffusion flux of water to the cathode, while optimum design in the cathode is more effective in the convective back-flow of water to the anode. Research is needed to investigate the effectiveness of the anode WML compared to the cathode WML, or vice versa.

Employing the concept of cathode WML, the substantial interrelation between water and methanol crossover in a DMFC fed with highly concentrated methanol solution was introduced by Bahrami and Faghri [17]. Back-flow of water, from the cathode to the anode, locally dilutes the methanol solution in the ACL and, therefore, reduces the methanol diffusion to the cathode. Methanol crossover is significantly alleviated by reducing the water crossover. The concept was investigated through both analytical and numerical models. It was reported that thickening the anode porous backing layer cannot reduce the significant methanol crossover without controlling the water transport. Fig. 9 illustrates the effect of using a cathode WML on the dilution of the methanol in the anode compared to the case without a WML. The methanol mass fraction in the ACL could not drop below 0.242, if a WML was not used, no matter how thick the anode backing layer was.

A proper model of water transport through the membrane depends on many factors, such as the capillary pressure and the liquid saturation at the catalyst layers (Eq. (30)) [53]. Most of the developed models employed the Leverett equation for the capillary pressure (Eq. (28)). Xu and Faghri [13] investigated the water and methanol transport inside the mixed-wet porous media by employing various experimentally measured mixed-wet capillary pressure and saturation relations (CPSR) rather than the conventional Leverett equation. Water transport predicted by the mixed-wet CPSR and the uniform-wet Leverett CPSR was compared. The significant dependence of water transport predictions on the employed capillary pressure relation was reported, emphasizing the requirement of future research regarding developing an appropriate capillary pressure relation for fuel cell applications.

5.2. Coupled heat and mass transport

Since the efficiency of DMFCs is low compared to that of hydrogen PEMFCs, more waste heat is expected in DMFCs than in hydrogen PEMFCs of equal power density. For instance, considering

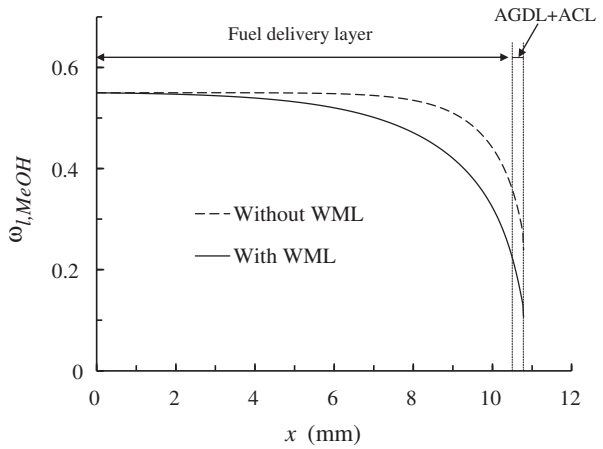

Fig. 9. The effect of using a water management layer (WML) in the cathode on the liquid methanol distribution in the anode (15 M solution in the reservoir and $\bar{I} = 1200\ \mathrm{A\,m^{-2}}$). Adopted from Ref. [17].

a 3 W passive DMFC operating at 20% efficiency, roughly 12 W of waste heat is produced which can potentially increase the cell temperature. Increasing the cell temperature has pros and cons. It is advantageous, as the higher temperature improves the MOR and ORR kinetics. Increase in temperature, however, facilitates unfavorable effects such as methanol and water evaporation and methanol and water crossover through the membrane.

There are four sources of heat generation in a DMFC: entropic heat of reactions (reversible heat), irreversible heat of reaction, ohmic loss (Joule heating), and the latent heat of phase change (condensation of water and methanol). The entropic heat is representative of entropy change for each half-cell reaction in the catalyst layers. The Peltier coefficient ($\prod_h$) is one of the most crucial parameters in calculating the local entropic heat transport, and is defined as follows:

$$\prod_h = T\frac{\Delta S}{nF} \tag{31}$$

The Peltier coefficient is experimentally measured for half-cell reactions, since the entropy of electrons is unknown. The Peltier coefficient for the ORR is −13 mV at 25 °C [158,159]. Due to the lack of experimental measurement of Peltier coefficient for the MOR, it may be approximated as:

$$\prod_{h,MOR} = \left(T\frac{\Delta S}{nF}\right)_{\text{Eq. (3)}} - \prod_{h,ORR} \tag{32}$$

The irreversibility of the electrochemical reactions (cathode and anode activation overpotentials) significantly contributes to the heat generation. Ohmic heat results from electronic and mostly from protonic current owing to a much lower ion conductivity of membrane relative to the electron conductivity of the carbon phase. Contribution of each of the four sources in total cell temperature depends on the operating conditions and the cell configuration. Neglecting the phase change for a hydrogen PEMFC, entropic, irreversible and ohmic heat generations roughly account for 55%, 35% and 10% of the total heat release, respectively [160].

Interplay between heat and water transport in a hydrogen PEMFC is discussed by several investigators [161–163]. In DMFCs, heat and mass transport are coupled through: (i) condensation and evaporation accompanied by heat release and adsorption, respectively, (ii) methanol and water transport due to the heat pipe effect, and (iii) temperature dependency of most transport properties such as the diffusion coefficient and the electroosmotic drag coefficient. The heat pipe effect refers to the mass transport due to evaporation from one point within the cell and condensation in other places.

Most macroscopic models developed for DMFCs are isothermal [3–6,8,15,19,20,49–53,59,63,65,73,121,123,127,128,144,145,150,164–167], while there are others considering the thermal effects [9,10,16,17,56–58,62,67,68,70]. To the authors' knowledge, Divisek et al. [62] was the first to introduce a DMFC model employing coupled heat–mass–charge transport equations. Although the governing equations were given in transient form and the coupling of all source terms to the temperature was shown, there were no results or discussions regarding either the transient behavior of the system or the temperature effect on transport phenomena. Chen and Zhao [126] provided a one-dimensional, non-isothermal model to analytically solve the heat and mass transport inside a passive DMFC. A closed-form solution for the temperature of the catalyst layers was the main contribution of this study. Similar analytical models were reported by others [117,168].

The temperature also has an indirect effect on the mass transfer though the kinetics of electrochemical reactions. A non-uniform temperature distribution in catalyst layers results in a non-uniform current density, which in turn results in non-uniform mass production in the catalyst layers. Bahrami and Faghri [16] developed a non-isothermal, two-phase model to compare a fully passive DMFC to a semi-passive one. It was reported that despite the negative effect of reduction in the cell temperature for the higher air flow rates in the cathode channel, it was beneficial since it created more uniform temperature and current density distributions along the catalyst layers. Fig. 10 depicts that as the air flow rate in the cathode channel reduces, the current density deviates more from a uniform distribution. This is primarily due to the non-uniform temperature distribution of the cell at lower air flow rates in the cathode channel.

Local methanol/water vapor partial pressure plays an important role in mass transfer between two phases and is a strong function of the temperature and porous structure. The dependency of partial pressure of condensable species on the pore size of the porous structure is usually overlooked. The average pore size ranges from 10 to 100 nm in catalyst layers [169], and from 1 to 100 μm in the GDLs [46]. The nanostructure of the pore network affects the mass transport by changing the local vapor pressures in these pores. For instance, the equilibrium water vapor pressure in a micro-pore of 20 nm increases by 11% at 25 °C and by 9% at 80 °C, compared to macrostructure [160]. This issue becomes more crucial when it comes to the fact that usually one of the catalyst layers experiences the highest temperature in the cell. As noted earlier, isothermal

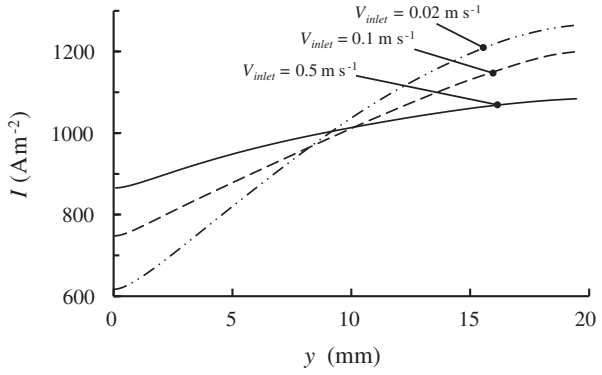

Fig. 10. The effect of air flow rate in the cathode channel on the current density distribution. Adopted from Ref. [117].

pore network models are developed for the catalyst layers and the GDLs mostly for hydrogen PEMFCs to capture the pore level, two-phase transport phenomena [36–46]. This type of modeling, including the temperature effects, is needed to delineate the effects of porous structure on the coupled heat and mass transport in DMFCs.

5.3. Enhanced system energy density

From the early stages of DMFC development, maintaining the merit of high system-level energy density was among the most prominent priorities. However, until the late 2000s, most of studies were focusing on understanding the underlying physics in transport phenomena in DMFCs. As noted earlier, a very dilute methanol (3–4 M) is conventionally supplied to the anode of a DMFC. To increase the energy density, concentrated methanol solution must be fed to the anode. Faghri et al. [8–10,12,16,17,56–58,67] were among the pioneers focusing on increasing the system-level energy density of DMFCs. Two approaches were undertaken to achieve the goal of utilizing concentrated methanol solution in the anode: (i) increasing the resistance against the liquid methanol flow to the anode, and (ii) change in the methanol feed phase. The latter approach achieved successful results in terms of experimental evidences [170,171].

5.3.1. Increasing the resistance against the liquid methanol

This approach was based on employing a porous medium between the pure methanol reservoir and the membrane electrode assembly. A WML in the cathode was used to passively supply water to the anode. Several detailed models were developed for this concept during the past six years. In the ideal case, methanol is stored in a porous fuel cartridge in contact with the main membrane electrode assembly. Rice and Faghri [8] established an isothermal, one-dimensional, transient, two-phase model for a liquid-feed passive DMFC, including the fuel delivery system. Pure liquid methanol was stored in a container and provided to the anode. Later, the temperature effect was added to the model [10]. The continuous and discontinuous phase limitations, as well as a probabilistic spread of the porous properties, were included into the macroscopic DMFC model. These added physical characteristics portrayed the departure of carbon dioxide from the anode side at preferential locations. Employing a model with the same features, Xiao and Faghri [58] investigated the transient change in the concentration of the methanol solution in the reservoir.

Later, Bahrami and Faghri [67] included the porous fuel cartridge saturated with pure methanol into a two-dimensional, transient, non-isothermal model. The transient operation of the fully passive DMFC was investigated. An equation for the dissolved water into the membrane phase was added to the model in order to precisely capture all water transport mechanisms through the membrane. It was shown that a cell using initially water-saturated porous layers at the anode can successfully operate with pure methanol, if a proper water supply from the cathode is provided. Fig. 11 illustrates the variation of methanol mass fraction in the fuel cartridge and the ACL over time. The fuel (methanol) in the cartridge is consumed during the normal operation of the DMFC. It was assumed that no dry-out occurs in the fuel cartridge during the cell operation. This assumption is a requirement difficult to meet in an experimental investigation, which led to a new approach for increasing the system-level energy density, described in the subsequent section.

5.3.2. Change in the methanol feed phase

This approach is known as vapor-feed technology. The vapor-feed terminology is not new and roots back to the early DMFC works that centered on achieving lower methanol crossover by using vaporized methanol solution via an external heat source. Early models for vapor-feed DMFCs were mostly single-phase. To the best of authors' knowledge, Scott et al. [118,172] and Dohle et al. [145] pioneered the study of charge and mass transfers in a vapor-feed DMFC through a one-dimensional, single-phase, semi-empirical model. Kulikovsky et al. [165] presented a two-dimensional, single-phase model for a vapor-feed DMFC without considering the methanol crossover through the membrane.

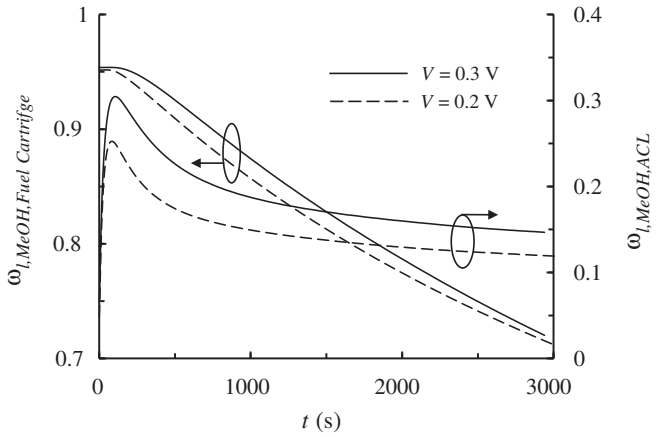

Fig. 11. The change in methanol mass fraction in the fuel cartridge, and the ACL with time. Adopted from Ref. [67].

Recently, efforts, mostly experimental, are directed at utilizing the concept of vapor-feed DMFC to improve the energy density of the system in a passive manner [9,12,57,112,171,173–178]. The common feature for this type of DMFC is the use of a passive vaporizer with no external power. Methanol is volatile with the boiling temperature of 64.5 °C at atmospheric pressure. It tends to evaporate easily even at room temperature. Various materials may be employed as a passive vaporizer, such as Nafion® membranes [170,171,174], porous carbon plates [112,173], silicone membranes [175,176], porous evaporation pads [177], and polydimethylsiloxane (PDMS) pervaporation membranes [178]. Utilizing an additional hydrophobic porous layer between the vaporizer and membrane electrolyte assembly prevents the condensation of methanol and water on the surface of vaporizer. This feature makes the passive vapor-feed DMFC functional at room temperature [170,171]. If the vaporizer itself is hydrophobic, there is no need for an additional hydrophobic layer [112,173].

Rice and Faghri [9] first developed a one-dimensional analytical model of the methanol transport from a reservoir of pure methanol to the fuel cell. Next, they investigated the fundamentals of a passive, vapor-feed DMFC using a transient, two-dimensional, two-phase, non-isothermal model. There was no evaporation pad in the model. However, a vapor chamber between the anode porous layers and the pure methanol distributor was considered in which only methanol vapor was allowed to exist. The back-flow of water to the methanol distributor was captured in this model. Xiao and Faghri [57] later investigated the transient characteristics of a passive vapor-feed DMFC using a model with the same feature, but with changes in the fuel cell configuration. An additional barrier layer, called the buffer layer, was considered between the vapor chamber and the anode porous layers. The evaporation/condensation phenomenon at the vaporizer was included. The methanol and water vapor concentrations across the vapor chamber were assumed constant. Xu and Faghri [12] developed a model in which the evaporation rate from a vaporizer was treated differently. The cell configuration considered in the model was very

close to what was experimentally built [170]. Based on the solution-diffusion model [179], the flow rate of the methanol vapor into the system was calculated. A hydrophobic vapor transport layer was employed between the AGDL and the vaporizer in which no condensation occurs. The rest of the domain, except for the membrane, was studied through a steady state, two-dimensional, two-phase, non-isothermal model. In a similar model developed by Yang et al. [64], various operating conditions of a vapor-feed DMFC working with pure methanol were discussed.

A transient, two-phase model was presented by Bahrami and Faghri [66] to investigate the major contributors to the transient response time of a passive vapor-feed DMFC upon applying a sudden load. Both the scale analysis and the predictions from the full numerical model revealed that the transient response time depends primarily on the cell load. At high current densities, mass consumption in the ACL becomes dominant in the cell transient response time, whereas at lower current densities, both the diffusive liquid transport in the anode and the mass consumption in the anode catalyst layers are predominant.

Note that none of above models developed for vapor-feed DMFCs fed with pure methanol was able to capture the decaying performance of the cell during operation time. This must be addressed in future research. This is mainly due to the lack of an accurate physical insight for the mass transfer through the membrane evaporator.

5.4. Start-up and transient operation

Change in operating conditions, such as sudden changes in the cell temperature, load or feed concentration, makes the cell undergo a transient operation. A fundamental understanding of the DMFC dynamic characteristics under transient operation conditions is essential in order to effectively design and control the system, especially for the practical applications where the load may constantly fluctuate. The other situation where the study of transient operation is of great importance is passive DMFCs with a finite amount of methanol in a reservoir. Nonetheless, there are few experimental studies reported in this regard. A widely accepted experimental approach is to make a step change in parameters such as current density [180–182] or methanol feed concentration [183,184] and then study the cell's response to this change.

There are several mathematical models developed to investigate the transient response of DMFCs [9,10,14,56–58,66,67,183,185–187]. Sundmacher et al. [183] showed that the voltage demonstrated an overshoot in response to a step change in the methanol feed concentration. Schultz et al. [185] revealed that this voltage overshoot originates from the different response time of the cathode and anode overpotentials to the change in the methanol concentration. In a different approach, Krewer et al. [186,187] studied the cell voltage response to a step change in the cell current density. They concluded that the anode reaction mechanism was the main physicochemical phenomenon causing the anode overpotential and cell voltage overshoots [186]. Consistent with the experimental results [182], it was reported that the methanol crossover is the dominating factor that causes the cathode overpotential and cell voltage overshoot [187]. Yang and Zhao [14] investigated the transient response of a passive DMFC to a sudden change in both the cell current density and the feeding concentration of methanol. It was shown that the double layer effects increase the transient response time to a sudden change of either cell current or the concentration of feed methanol.

All of the above studies focus on DMFCs fed with a dilute methanol solution. Faghri et al. [8–10,57,58,66,67] developed transient models for passive DMFCs using highly concentrated methanol. Rice and Faghri [8,10] proposed a transient model for a DMFC constantly fed with pure methanol from a reservoir. Later, Xiao and Faghri [58] considered the change in the reservoir methanol concentration as the boundary condition in the anode in order to estimate the running time of the system. Bahrami and Faghri [67] investigated the transient change of methanol concentration of a porous fuel cartridge (Fig. 11). Recently, a numerical model including a scale analysis was employed by Bahrami and Faghri [66] to show the dependency of the transient response time of a vapor-feed DMFC.

6. Unresolved issues

During the past decade, considerable advancements in predicting capabilities of the coupled charge–energy-species transport phenomena in DMFCs have been achieved through macroscopic models. It is believed that the focus of future DMFC modeling studies should be centered in: (i) a better understanding of the reaction kinetics of methanol crossover in the cathode, (ii) transport phenomena in vapor-feed DMFCs using pure methanol, (iii) cold start-up of a DMFC, and (iv) providing a general capillary pressure using pore-scale models. More details regarding the aforementioned items are presented below.

No matter what controlling method is implemented, methanol crossover remains a crucial issue for DMFCs. A better understanding of the underlying physics for the methanol reaction in the CCL and its effect on the mixed potential is imperative. As the Pt catalyst in the CCL is not methanol tolerant, methanol in the cathode reacts with oxygen to produce heat, without generating electricity. The simultaneous competition of methanol and oxygen on occupying a specific catalyst surface must be taken into account in order to develop a proper kinetics for the MOR in the CCL. The other challenging issue is the Pt poisoning in the CCL as a result of methanol crossover. According to recent experimental evidences [26], cathode overpotential spikes at a certain methanol crossover rate, caused mainly by the Pt poisoning.

Vapor-feed technology for DMFC demonstrated a promising performance and opened a new horizon in utilizing a high concentration methanol solution in the anode of a DMFC. This technology can be used for other liquid-fed fuel cells, such as direct ethanol fuel cells with some minor modifications. The current physical models, however, are not able to completely predict the proper transport phenomena in a vapor-feed DMFC. Experiments showed that the performance (P, W m^{-2}) of vapor-feed DMFCs utilizing the membrane vaporizer decreases with time. None of the available models are able to predict this behavior. It is believed that this is primarily due to lack of physical insight regarding the mass transfer through the vaporizer, usually a polymer membrane, and requires special treatment.

A rapid and successful cold start-up in freezing temperature conditions is of great importance for DMFCs. However, the subject attracted the least attention during past two decades. This is due in part to the presence of methanol with low freezing point (−97.78 °C for pure methanol) in the anode. The presence of methanol, even at small mass fractions, significantly reduces the freezing point of the solution. The anode side of DMFCs is therefore less vulnerable against the freezing than the cathode side. There is a significant amount of water in the cathode side both from the electrochemical reaction and the water crossover. Migrated methanol to the cathode is most likely oxidized in the CCL. Research must be conducted to evaluate the potential freezing of water in the cathode and blocking the reactive catalyst sites in the CCL.

Although some efforts have been made to provide an empirical capillary pressure for fuel cells applications, the Leverett function is still most widely used. This relation is not appropriate for the porous mixed-wet structure of DMFCs where both hydrophilic and

hydrophobic pores are randomly distributed. The liquid saturation calculated from the capillary pressure has a significant effect on the accurate prediction of transport phenomena such as methanol crossover, water crossover, temperature distribution and evaporation/condensation of species. Micro-scale models, such as PNM, are expected to provide a general capillary pressure relation as a function of liquid saturation, porosity, structure of porous medium, and the degree of hydrophobicity. The model may be developed for common GDL materials, such as carbon paper and carbon cloth. For this purpose, a randomly generated contact angle function, representative of the mixed-wettability of the GDL, should be fed to the model to match the average percentage of added PTFE to the GDL. Experimental evaluation of the PTFE distribution is of urgent importance in order to have more accurate predictions out of the pore-scale modeling. The effect of mixed-wettability of the porous structure on the water and methanol transport should also be investigated. One other area that requires future research is including temperature effects in two-phase PNM for transport phenomena in the catalyst layers and the GDLs. Currently, all of the developed two-phase PNMs are isothermal and neglect the temperature effect on mass transport.

7. Conclusions

A critical review of DMFC numerical models is presented. Numerical models are classified based on the most challenging issues regarding the transport phenomena in DMFCs. Differences between various common modeling methodologies and approaches are briefly explained. While significant advancements in macroscopic DMFC modeling have been achieved during the past decade, there are still areas requiring urgent research. Due to the dependency of various transport variables on capillary pressure, a constitutive relation of capillary pressure accounting for the mixed-wet porous structure is needed. This can be achieved through an advanced pore-scale modeling. Passive vapor-feed technology in DMFCs has demonstrated a promising performance during the past couple of years. However, an in-depth explanation of mass transport though a passive vaporizer, usually a membrane, is lacking.

Nomenclature

a	specific catalyst area, m^{-1}
A	frequency factor
A_{lg}	interfacial specific area between liquid and gas phases, m^{-1}
ACL	anode catalyst layer
AGDL	anode gas diffusion layer
C	molar concentration, mol m^{-3}
C_p	specific heat capacity, J kg^{-1} K^{-1}
CCL	cathode catalyst layer
CGDL	cathode gas diffusion layer
D	diffusivity, m^2 s^{-1}
DMFC	direct methanol fuel cell
E_A	activation energy, J
F	Faraday constant, 96485.3 A s mol^{-1}
G	Gibbs free energy, J
h_{fg}	heat of vaporization, J kg^{-1}
h_{lg}	interfacial transfer rate constant for methanol, m^2 s^{-1}
I	current density, A m^{-2}
J	reaction rate, A m^{-3}
J_o	exchange current density, A m^{-2}
K	permeability of porous media, m^2
k	thermal conductivity, W m^{-2} K^{-1}/reaction rate constant/permeability
k_c	condensation rate, s^{-1}
k_e	evaporation rate, Pa^{-1} s^{-1}
K	reaction constant
k_r	relative permeability
M	molecular weight, kg mol^{-1}
M^2	multiphase mixture
$\dot{m}$	mass flow rate, kg s^{-1}
MFM	multi-fluid multiphase
MOR	methanol oxidation reaction
n	number of electrons
$\dot{n}$	molar flow rate, mol s^{-1}
ORR	oxygen reduction reaction
p	pressure, Pa
PEM	polymer electrolyte membrane
PEMFC	PEM fuel cell
PNM	pore network modeling
Pt	platinum
R	reaction rate, A m^{-2}
R_u	Universal gas constant, 8.31446 J mol^{-1} K^{-1}
Ru	Ruthenium
$\dot{S}$	source term
S	entropy, J mol^{-1} K^{-1}
s	liquid saturation
t	time, s
T	temperature, K
V	voltage, V/mass-averaged velocity, m s^{-1}
$\widehat{V}$	molar-averaged velocity, m s^{-1}
WML	water management layer
x	mole fraction

Greek

α	transfer coefficient
Γ	diffusion coefficient, m^2 s^{-1}/kinetics constant, mol m^{-3}
ε	porosity
η	overpotential, V
θ	catalyst surface coverage fraction/contact angel
κ_H	Henry's constant, Pa
λ	water content
μ	viscosity, kg m^{-1} s^{-1}
σ	conductivity, Ω^{-1} m^{-1}
ϕ	potential, V
ω	mass fraction
Π	Peltier coefficient, V

Superscripts

eff	effective value
eq	equilibrium
g	gas
H_2O	water
l	liquid
m	mixture
mem	membrane
lat	latent
MeOH	methanol
osm	electroosmotic
reac	electrochemical reaction
ref	reference
sat	saturation
Max-Stef	Maxwell–Stefan

Subscripts

a	anode
c	cathode/capillary/carbon phase
dw	dissolved water
e	electron

g	gas phase
i	index number for species
l	liquid
m	mass/membrane
N	number of components
p	pressure
ox	oxidation
red	reduction
sat	saturation
T	temperature
v	vapor

References

[1] B.L. García-Díaz, J.R. Patterson, J.W. Weidner, J. Fuel Cell Sci. Technol. 9 (2012).
[2] A.J. Bard, L.R. Faulkner, Electrochemical Methods, Fundamentals and Applications, second ed., John Wiley & Sons, NJ, USA, 2001.
[3] W.W. Yang, T.S. Zhao, J. Power Sources 174 (2007) 136–147.
[4] W.W. Yang, T.S. Zhao, Electrochim. Acta 52 (2007) 6125–6140.
[5] W.W. Yang, T.S. Zhao, Y.L. He, J. Power Sources 185 (2008) 765–775.
[6] C. Xu, T.S. Zhao, W.W. Yang, J. Power Sources 178 (2008) 291–308.
[7] Z.H. Wang, C.Y. Wang, J. Electrochem. Soc. 150 (2003) A508–A519.
[8] J. Rice, A. Faghri, Int. J. Heat Mass Transf. 49 (2006) 4804–4820.
[9] J. Rice, A. Faghri, Int. J. Heat Mass Transf. 51 (2008) 948–959.
[10] J. Rice, A. Faghri, J. Heat Transf. 130 (2008) 062001.
[11] C. Xu, A. Faghri, Int. J. Heat Mass Transf. 53 (2010) 1951–1966.
[12] C. Xu, A. Faghri, J. Power Sources 195 (2010) 7011–7024.
[13] C. Xu, A. Faghri, J. Fuel Cell Sci. Technol. 7 (2010).
[14] W.W. Yang, T.S. Zhao, J. Power Sources 185 (2008) 1131–1140.
[15] W.W. Yang, T.S. Zhao, C. Xu, Electrochim. Acta 53 (2007) 853–862.
[16] H. Bahrami, A. Faghri, Int. J. Heat Mass Transf. 53 (2010) 2563–2578.
[17] H. Bahrami, A. Faghri, J. Fuel Cell Sci. Technol. 8 (2011).
[18] Y. Sun, L. Xing, K. Scott, J. Power Sources 195 (2010) 1–10.
[19] J.P. Meyers, J. Newman, J. Electrochem. Soc. 149 (2002) A718–A728.
[20] J. Nordlund, G. Lindbergh, J. Electrochem. Soc. 149 (2002) A1107–A1113.
[21] M.R. Shivhare, R.G. Allen, K. Scott, A.J. Morris, E.B. Martin, J. Electroanal. Chem. 595 (2006) 145–151.
[22] D. Kareemulla, S. Jayanti, J. Power Sources 188 (2009) 367–378.
[23] A. Hamnett, Catal. Today 38 (1997) 445–457.
[24] H.A. Gaisteiger, N. Markovic, P.N. Ross Jr., P.N.J. Cairns, J. Phys. Chem. 97 (1993) 12020–12029.
[25] Z. Miao, Y. He, X. Li, J. Zou, J. Power Sources 185 (2008) 1233–1246.
[26] T. Tamaki, A. Yamauchi, T. Ito, H. Ohashi, T. Yamaguchi, Fuel Cells 11 (2011) 394–403.
[27] Q. Wang, M. Eikerling, D. Song, Z. Liu, J. Electroanal. Chem. 573 (2004) 61–69.
[28] M. Eikerling, J. Electrochem. Soc. 153 (2006) E58–E70.
[29] W. Sun, B.A. Peppley, K. Karan, Electrochim. Acta 50 (2005) 3359–3374.
[30] S. Kamarajugadda, S. Mazumder, J. Power Sources 183 (2008) 629–642.
[31] M. Secanell, K. Karan, A. Suleman, N. Djilali, Electrochim. Acta 52 (2007) 6318–6337.
[32] M. Secanell, B. Carnes, A. Suleman, N. Djilali, Electrochim. Acta 52 (2007) 2668–2682.
[33] J. Liu, M. Eikerling, Electrochim. Acta 53 (2008) 4435–4446.
[34] G. Wang, P.P. Mukherjee, C. Wang, Electrochim. Acta 52 (2007) 6367–6377.
[35] M. El Hannach, J. Pauchet, M. Prat, Electrochim. Acta 56 (2011) 10796–10808.
[36] P.K. Sinha, C. Wang, Electrochim. Acta 52 (2007) 7936–7945.
[37] P.K. Sinha, C. Wang, Chem. Eng. Sci. 63 (2008) 1081–1091.
[38] P.K. Sinha, P.P. Mukherjee, C.-Y. Wang, J. Mater. Chem. 17 (2007) 3089–3103.
[39] J.T. Gostick, M.A. Ioannidis, M.W. Fowler, M.D. Pritzker, J. Power Sources 173 (2007) 277–290.
[40] B. Markicevic, A. Bazylak, N. Djilali, J. Power Sources 171 (2007) 706–717.
[41] A. Bazylak, V. Berejnov, B. Markicevic, D. Sinton, N. Djilali, Electrochim. Acta 53 (2008) 7630–7637.
[42] T. Koido, T. Furusawa, K. Moriyama, J. Power Sources 175 (2008) 127–136.
[43] K. Lee, J.H. Nam, C. Kim, Electrochim. Acta 54 (2009) 1166–1176.
[44] K. Lee, J.H. Nam, C. Kim, J. Power Sources 195 (2010) 130–141.
[45] L. Ceballos, M. Prat, J. Power Sources 195 (2010) 825–828.
[46] G. Luo, Y. Ji, C. Wang, P.K. Sinha, Electrochim. Acta 55 (2010) 5332–5341.
[47] R. Wu, X. Zhu, Q. Liao, H. Wang, Y. Ding, J. Li, D. Ye, Electrochim. Acta 55 (2010) 7394–7403.
[48] T.J. Dursch, M.A. Ciontea, C.J. Radke, A.Z. Weber, Langmuir 28 (2012) 1222–1234.
[49] E. Birgersson, J. Nordlund, M. Vynnycky, C. Picard, G. Lindbergh, J. Electrochem. Soc. 151 (2004) A2157–A2172.
[50] E. Birgersson, J. Nordlund, H. Ekström, M. Vynnycky, G. Lindbergh, J. Electrochem. Soc. 150 (2003) A1368–A1376.
[51] V.A. Danilov, J. Lim, I. Moon, H. Chang, J. Power Sources 162 (2006) 992–1002.
[52] F. Liu, C.Y. Wang, J. Electrochem. Soc. 154 (2007) B514–B522.
[53] W. Liu, C.Y. Wang, J. Electrochem. Soc. 154 (2007) B352–B361.
[54] J. Ge, H. Liu, J. Power Sources 163 (2007) 907–915.
[55] T.Z. Yan, T.C. Jen, Int. J. Heat Mass Transf. 51 (2008) 1192–1204.
[56] B. Xiao, H. Bahrami, A. Faghri, J. Power Sources 195 (2010) 2248–2259.
[57] B. Xiao, A. Faghri, Int. J. Heat Mass Transf. 52 (2009) 3525–3533.
[58] B. Xiao, A. Faghri, Int. J. Heat Mass Transf. 51 (2008) 3127–3143.
[59] C.E. Shaffer, C.Y. Wang, Electrochim. Acta 54 (2009) 5761–5769.
[60] C.E. Shaffer, C.Y. Wang, ECS Trans. 16 (2008) 1507–1518.
[61] J.J. Garvin, J.P. Meyers, J. Electrochem. Soc. 158 (2011) B1119–B1127.
[62] J. Divisek, J. Fuhrmann, K. Gärtner, R. Jung, J. Electrochem. Soc. 150 (2003) A811–A825.
[63] G. Murgia, L. Pisani, A.K. Shukla, K. Scott, J. Electrochem. Soc. 150 (2003) A1231–A1245.
[64] W.W. Yang, T.S. Zhao, Q.X. Wu, Int. J. Hydrogen Energy 36 (2011) 6899–6913.
[65] W.W. Yang, T.S. Zhao, J. Power Sources 188 (2009) 433–446.
[66] H. Bahrami, A. Faghri, Int. J. Hydrogen Energy 37 (2012) 8641–8658.
[67] H. Bahrami, A. Faghri, J. Electrochem. Soc. 157 (2010) B1762–B1776.
[68] R. Chen, T.S. Zhao, W.W. Yang, C. Xu, J. Power Sources 175 (2008) 276–287.
[69] C. Xu, A. Faghri, J. Power Sources 196 (2011) 6332–6346.
[70] Z. Miao, Y.L. He, J.Q. Zou, J. Power Sources 195 (2010) 3693–3708.
[71] Y. He, Z. Miao, T. Zhao, W. Yang, Int. J. Hydrogen Energy 37 (2012) 4422–4438.
[72] D. Natarajan, T. Van Nguyen, J. Electrochem. Soc. 148 (2001) a1324–a1335.
[73] W. Liu, C.Y. Wang, J. Power Sources 164 (2007) 189–195.
[74] C.E. Shaffer, C.Y. Wang, J. Power Sources 195 (2010) 4185–4195.
[75] C.Y. Wang, P. Cheng, Int. J. Heat Mass Transf. 39 (1996) 3607–3618.
[76] P. Cheng, C.Y. Wang, Int. J. Heat Mass Transf. 39 (1996) 3619–3632.
[77] C.Y. Wang, C. Beckermann, Int. J. Heat Mass Transf. 36 (1993) 2747–2758.
[78] A. Faghri, Y. Zhang, Transport Phenomena in Multiphase Systems, Elsevier Inc., Burlington, MA, 2006.
[79] K.S. Udell, Int. J. Heat Mass Transf. 28 (1985) 485–495.
[80] A.Z. Weber, R.M. Darling, J. Newman, J. Electrochem. Soc. 151 (2004) A1715–A1727.
[81] M. Acosta, C. Merten, G. Eigenberger, H. Class, R. Helmig, B. Thoben, H. Müller-Steinhagen, J. Power Sources 159 (2006) 1123–1141.
[82] K.G. Gallagher, R.M. Darling, T.W. Patterson, M.L. Perry, J. Electrochem. Soc. 155 (2008) B1225–B1231.
[83] T.V. Nguyen, G. Lin, H. Ohn, X. Wang, Electrochem. Solid-State Lett. 11 (2008) B127–B131.
[84] Q. Ye, T. Van Nguyen, J. Electrochem. Soc. 154 (2007) B1242–B1251.
[85] X. Wang, T. Van Nguyen, J. Electrochem. Soc. 155 (2008) B1085–B1092.
[86] M.M. Verbrugge, J. Electrochem. Soc. 136 (1989) 417–423.
[87] S. Nam, S. Kim, Y. Kang, J.W. Lee, K. Lee, J. Membr. Sci. 322 (2008) 466–474.
[88] A.S. Aricò, V. Baglio, V. Antonucci, I. Nicotera, C. Oliviero, L. Coppola, P.L. Antonucci, J. Membr. Sci. 270 (2006) 221–227.
[89] Y. Lin, C. Yen, C. Hung, Y. Hsiao, C.M. Ma, J. Power Sources 168 (2007) 162–166.
[90] H. Tang, M. Pan, S. Jiang, Z. Wan, R. Yuan, Colloids Surf. Physicochem. Eng. Aspects 262 (2005) 65–70.
[91] S.R. Yoon, G.H. Hwang, W.I. Cho, I.-H. Oh, S.-A. Hong, H.Y. Ha, J. Power Sources 106 (2002) 215–223.
[92] Y. Kim, K. Park, J. Choi, I. Park, Y. Sung, Electrochem. Commun. 5 (2003) 571–574.
[93] T. Hejze, B.R. Gollas, R.K. Sauerbrey, M. Schmied, F. Hofer, J.O. Besenhard, J. Power Sources 140 (2005) 21–27.
[94] L. Brandão, J. Rodrigues, L.M. Madeira, A. Mendes, Int. J. Hydrogen Energy 35 (2010) 11561–11567.
[95] K.N.T. Do, D. Kim, J. Appl. Polym. Sci. 110 (2008) 1763–1770.
[96] R. Fu, D. Julius, L. Hong, J. Lee, J. Membr. Sci. 322 (2008) 331–338.
[97] S. Fei, R.M. Wood, D.K. Lee, D.A. Stone, H. Chang, H.R. Allcock, J. Membr. Sci. 320 (2008) 206–214.
[98] W. Li, A. Bellay, Y.-Z. Fu, A. Manthiram, J. Power Sources 180 (2008) 719–723.
[99] A.K. Sahu, G. Selvarani, S. Pitchumani, P. Sridhar, A.K. Shukla, N. Narayanan, A. Banerjee, N. Chandrakumar, J. Electrochem. Soc. 155 (2008) B686–B695.
[100] H. Lin, C. Zhao, W. Ma, H. Li, H. Na, Int. J. Hydrogen Energy 34 (2009) 9795–9801.
[101] D. Chu, S. Gilman, J. Electrochem. Soc. 141 (1994) 1770–1773.
[102] P.S. Kauranen, E. Skou, J. Electroanal. Chem. 408 (1996) 189–198.
[103] V. Gogel, T. Frey, Z. Yongsheng, K.A. Friedrich, L. Jörissen, J. Garche, J. Power Sources 127 (2004) 172–180.
[104] J. Han, H. Liu, J. Power Sources 164 (2007) 166–173.
[105] J. Chung, S. Heo, S. Song, J. Kim, S. Kang, K. Choi, Jpn. J. Appl. Phys. 49 (2010).
[106] A. Heinzel, V.M. Barragán, J. Power Sources 84 (1999) 70–74.
[107] R. Jiang, D. Chu, J. Electrochem. Soc. 151 (2004) A69–A76.
[108] M. Ahmed, I. Dincer, Int. J. Energy Res. 35 (2011) 1213–1228.
[109] X. Ren, T.E. Springer, S. Gottesfeld, J. Electrochem. Soc. 147 (2000) 92–98.
[110] J.G. Liu, T.S. Zhao, Z.X. Liang, R. Chen, J. Power Sources 153 (2006) 61–67.
[111] G.Q. Lu, C.Y. Wang, T.J. Yen, X. Zhang, Electrochim. Acta 49 (2004) 821–828.
[112] M. Ali Abdelkareem, N. Nakagawa, J. Power Sources 162 (2006) 114–123.
[113] F. Liu, G. Lu, C.-Y. Wang, J. Electrochem. Soc. 153 (2006) A543–A553.
[114] N. Nakagawa, M.A. Abdelkareem, K. Sekimoto, J. Power Sources 160 (2006) 105–115.
[115] B. Garcia, V. Sethuraman, J.W. Weidner, R. Dougal, R.E. White, J. Fuel Cell Sci. Technol. 1 (2004) 43–48.

[116] A.A. Kulikovsky, Electrochem. Commun. 5 (2003) 530–538.
[117] H. Bahrami, A. Faghri, J. Power Sources 196 (2011) 1191–1204.
[118] K. Scott, W. Taama, J. Cruickshank, J. Power Sources 65 (1997) 159–171.
[119] S. Eccarius, B.L. Garcia, C. Hebling, J.W. Weidner, J. Power Sources 179 (2008) 723–733.
[120] N.S. Rosenthal, S.A. Vilekar, R. Datta, J. Power Sources 206 (2012) 129–143.
[121] J.P. Meyers, J. Newman, J. Electrochem. Soc. 149 (2002) A729–A735.
[122] S.S. Sandhu, R.O. Crowther, J.P. Fellner, Electrochim. Acta 50 (2005) 3985–3991.
[123] A.A. Kulikovsky, J. Appl. Electrochem. 30 (2000) 1005–1014.
[124] A.A. Kulikovsky, Electrochem. Commun. 4 (2002) 939–946.
[125] J. Ko, G. Lee, Y. Choi, P. Chippar, K. Kang, H. Ju, J. Power Sources 196 (2011) 935–945.
[126] R. Chen, T.S. Zhao, J. Power Sources 152 (2005) 122–130.
[127] A.A. Kulikovsky, J. Electrochem. Soc. 152 (2005) A1121–A1127.
[128] A.A. Kulikovsky, Electrochim. Acta 62 (2012) 185–191.
[129] H. Kim, J. Oh, J. Kim, H. Chang, J. Power Sources 162 (2006) 497–501.
[130] C. Xu, T.S. Zhao, J. Power Sources 168 (2007) 143–153.
[131] X. Ren, W. Henderson, S. Gottesfeld, J. Electrochem. Soc. 144 (1997) L267–L270.
[132] A. Oedegaard, C. Hentschel, J. Power Sources 158 (2006) 177–187.
[133] G.Q. Lu, F.Q. Liu, C.-Y. Wang, Electrochem. Solid-State Lett. 8 (2005) A1–A4.
[134] Q.X. Wu, S.Y. Shen, Y.L. He, T.S. Zhao, Int. J. Hydrogen Energy 37 (2012) 5958–5968.
[135] Q.X. Wu, T.S. Zhao, Int. J. Hydrogen Energy 36 (2011) 5644–5654.
[136] G. Jewett, Z. Guo, A. Faghri, J. Power Sources 168 (2007) 434–446.
[137] T. Schultz, K. Sundmacher, J. Membr. Sci. 276 (2006) 272–285.
[138] J. St-Pierre, J. Electrochem. Soc. 154 (2007) B88–B95.
[139] Z. Zhang, K. Promislow, J. Martin, H. Wang, B.J. Balcom, J. Power Sources 196 (2011) 8525–8530.
[140] M. Eikerling, Y.I. Kharkats, A.A. Kornyshev, Y.M. Volfkovich, J. Electrochem. Soc. 145 (1998) 2684–2699.
[141] I. Nazarov, K. Promislow, J. Electrochem. Soc. 154 (2007) B623–B630.
[142] T.E. Springer, T.A. Zawodzinski, S. Gottesfeld, J. Electrochem. Soc. 138 (1991) 2334–2342.
[143] A.Z. Weber, J. Newman, AIChE J. 50 (2004) 3215–3226.
[144] J.P. Meyers, J. Newman, J. Electrochem. Soc. 149 (2002) A710–A717.
[145] H. Dohle, J. Divisek, R. Jung, J. Power Sources 86 (2000) 469–477.
[146] H. Meng, C.-Y. Wang, J. Electrochem. Soc. 151 (2004) A358–A367.
[147] H. Meng, C. Wang, Chem. Eng. Sci. 59 (2004) 3331–3343.
[148] G. Lin, T. Van Nguyen, J. Electrochem. Soc. 153 (2006) A372–A382.
[149] H. Meng, Power Sources 162 (2006) 426–435.
[150] A.A. Kulikovsky, J. Electrochem. Soc. 150 (2003) A1432–A1439.
[151] A. Vorobev, O. Zikanov, T. Shamim, J. Power Sources 166 (2007) 92–103.
[152] N.P. Siegel, M.W. Ellis, D.J. Nelson, M.R. von Spakovsky, J. Power Sources 115 (2003) 81–89.
[153] A.A. Shah, G.-. Kim, W. Gervais, A. Young, K. Promislow, J. Li, S. Ye, J. Power Sources 160 (2006) 1251–1268.
[154] A.A. Shah, G.-S. Kim, P.C. Sui, D. Harvey, J. Power Sources 163 (2007) 793–806.
[155] E. Peled, A. Blum, A. Aharon, M. Philosoph, Y. Lavi, Electrochem. Solid-State Lett. 6 (2003) A268–A271.
[156] A. Blum, T. Duvdevani, M. Philosoph, N. Rudoy, E. Peled, J. Power Sources 117 (2003) 22–25.
[157] F. Liu, C.-Y. Wang, Electrochim. Acta 53 (2008) 5517–5522.
[158] Z. Jiang, J. Zhang, L. Dong, J. Zhuang, J. Electroanal. Chem. 469 (1999) 1–10.
[159] S. Shibata, M.P. Sumino, J. Electroanal. Chem. Interfacial Electrochem. 193 (1985) 135–143.
[160] S.G. Kandlikar, Z. Lu, Appl. Therm. Eng. 29 (2009) 1276–1280.
[161] A.Z. Weber, J. Newman, J. Electrochem. Soc. 153 (2006) A2205–A2214.
[162] N. Djilali, D. Lu, Int. J. Therm. Sci. 41 (2002) 29–40.
[163] Y. Wang, C.-Y. Wang, J. Electrochem. Soc. 153 (2006) A1193–A1200.
[164] S.F. Baxter, V.S. Battaglia, R.E. White, J. Electrochem. Soc. 146 (1999) 437–447.
[165] A.A. Kulikovsky, J. Divisek, A.A. Kornyshev, J. Electrochem. Soc. 147 (2000) 953–959.
[166] A.A. Kulikovsky, Electrochem. Commun. 4 (2002) 318–323.
[167] J. Ge, H. Liu, J. Power Sources 160 (2006) 413–421.
[168] V.B. Oliveira, D.S. Falcão, C.M. Rangel, A.M.F.R. Pinto, Int. J. Hydrogen Energy 33 (2008) 3818–3828.
[169] M. Uchida, Y. Aoyama, N. Eda, A. Ohta, J. Electrochem. Soc. 142 (1995) 4143–4149.
[170] C. Xu, A. Faghri, X. Li, J. Electrochem. Soc. 157 (2010) B1109–B1117.
[171] X. Li, A. Faghri, J. Power Sources 196 (2011) 6318–6324.
[172] K. Scott, W. Taamaa, J. Cruickshank, J. Appl. Electrochem. 28 (1998) 289–297.
[173] M.A. Abdelkareem, N. Morohashi, N. Nakagawa, J. Power Sources 172 (2007) 659–665.
[174] H. Kim, J. Power Sources 162 (2006) 1232–1235.
[175] X. Ren, J.J. Becerra, R.S. Hirsch, S. Gottesfeld, F.W. Kovacs, K.J. Shufon, Controlled Direct Liquid Injection Vapor Feed for a DMFC (2005).
[176] X. Ren, F.W. Kovacs, K.J. Shufon, S. Gottesfeld, Passive Water Management Techniques in Direct Methanol Fuel Cells (2008).
[177] Z. Guo, A. Faghri, J. Power Sources 167 (2007) 378–390.
[178] S. Eccarius, F. Krause, K. Beard, C. Agert, J. Power Sources 182 (2008) 565–579.
[179] L. Li, Z. Xiao, S. Tan, L. Pu, Z. Zhang, J. Membr. Sci. 243 (2004) 177–187.
[180] P. Argyropoulos, K. Scott, W.M. Taama, Electrochim. Acta 45 (2000) 1983–1998.
[181] P. Argyropoulos, K. Scott, W.M. Taama, J. Power Sources 87 (2000) 153–161.
[182] J. Kallo, J. Kamara, W. Lehnert, R. von Helmolt, J. Power Sources 127 (2004) 181–186.
[183] K. Sundmacher, T. Schultz, S. Zhou, K. Scott, M. Ginkel, E.D. Gilles, Chem. Eng. Sci. 56 (2001) 333–341.
[184] S. Zhou, T. Schultz, M. Peglow, K. Sundmacher, Phys. Chem. Chem. Phys. 3 (2001) 347–355.
[185] T. Schultz, U. Krewer, K. Sundmacher, J. Power Sources 165 (2007) 138–151.
[186] U. Krewer, A. Kamat, K. Sundmacher, J. Electroanal. Chem. 609 (2007) 105–119.
[187] U. Krewer, K. Sundmacher, J. Power Sources 154 (2006) 153–170.
[188] M. Vera, J. Power Sources 171 (2007) 763–777.